Title

STUDIES OF ADSORPTION AT WELL-OEDERED ELECTRODE SURFACES USING LOW ENERGY ELECTRON DIFFRACTION

Author

Ross, P.N.

Publication Date

1981-10-01

Lawrence Berkeley Laboratory
UNIVERSITY OF CALIFORNIA

Materials & Molecular
Research Division

Presented at the 5th International Summer Institute for Surface Sciences, University of Wisconsin, Milwaukee, WI, August 23-28, 1981, and to be published in the Proceedings, R. Howe and R. Vanselow, eds., Springer-Verlag, Berlin, W. Germany, 1982

STUDIES OF ADSORPTION AT WELL-ORDERED ELECTRODE SURFACES USING LOW ENERGY ELECTRON DIFFRACTION

Philip N. Ross, Jr.

October 1981

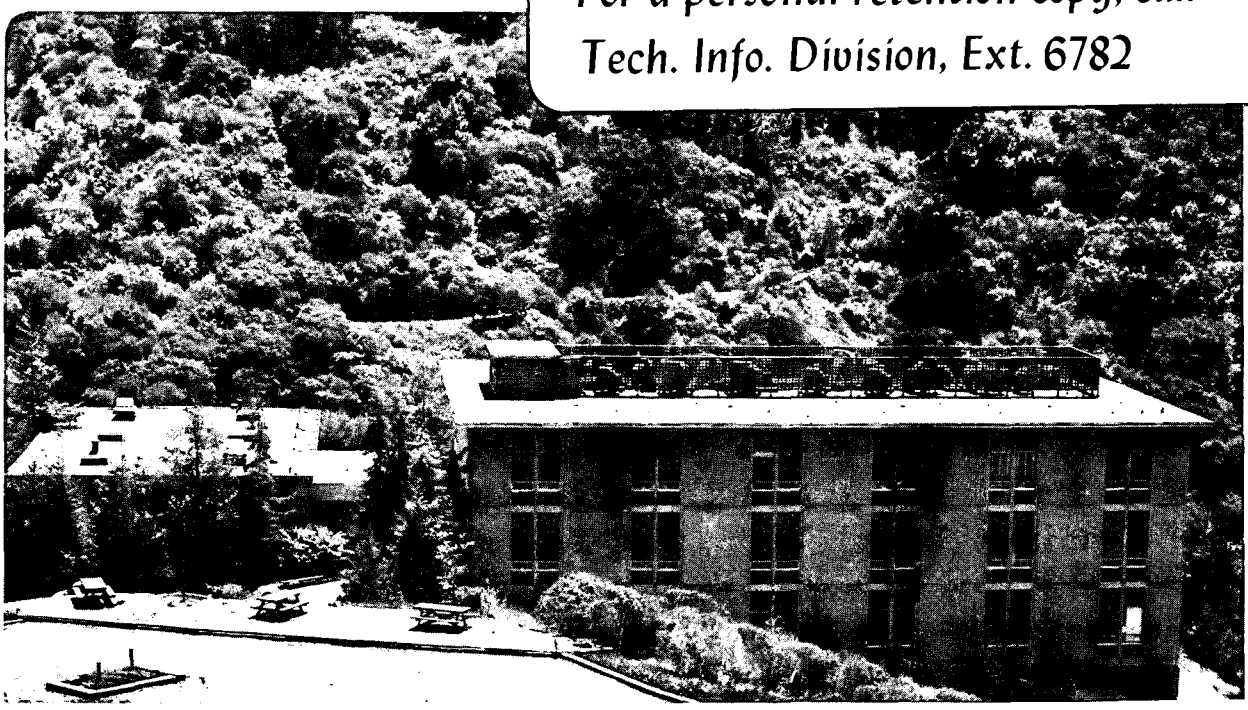

Prepared for the U.S. Department of Energy under Contract W-7405-ENG-48

DISCLAIMER

STUDIES OF ADSORPTION AT WELL-ORDERED ELECTRODE SURFACES USING LOW ENERGY ELECTRON DIFFRACTION

Philip N. Ross, Jr.

Lawrence Berkeley Laboratory
Materials and Molecular Research Division
University of California
Berkeley, California 94720

1. Introduction

As in gas-solid heterogeneous catalysis, the adsorbed intermediate plays a central role in the development of a quantitative theory for electrocatalysis. The geometric structure and the electronic and vibrational states of the adsorbate must be known in order to derive quantum mechanical descriptions of electron transfer occurring during adsorption of an electroactive species from solution, e.g. the electrodeposition of metals. There are electrochemical reactions where the rate determining step is not an electron transfer step, but a purely chemical step, such as chemisorption. This is the case, for example, in the classic hydrogen electrode reaction, $H_2 \rightarrow 2H^+ + 2e^-$, where for the Pt group metals the rate is determined by the rate of dissociative chemisorption of hydrogen. In reactions of this type, one is seeking virtually identical information about the adsorbed state as in heterogeneous catalysis, with the additional complication of the solution phase. Thus, studies of adsorbed states have the same important relationship to physical understanding of reaction paths and kinetics in both gas-solid and electrochemical catalysis.

The use of in-situ spectroscopic techniques to probe adsorbed intermediates is at the forefront of gas-solid catalytic research. Analogously, there are in-situ methods which have been used with

electrochemical systems to probe the geometric and electronic structure of adsorbates on electrode surfaces. Examples of these techniques are reflectance spectroscopy, ellipsometry and surface enhanced Raman spectroscopy (SERS). SERS seems to have the most promise of any of the in-situ techniques and was a lecture topic at the 1979 ISISS (1). The in-situ techniques suffer from a variety of shortcomings. All lack a general applicability and none provide, even in principle, a definitive determination of adsorbate structure. A number of research groups that study the electrode-electrolyte interface have developed ex-situ methods for this study, and it is these we shall concern ourselves with here. X-ray photoelectron spectroscopy (XPS) has been used extensively for ex-situ analysis of electrode surfaces (2) but not for the study of adsorbed or submonolayer electrodeposited species. In this review, we shall describe in some detail studies of submonolayer structures on electrode surfaces using the combination of classical electrochemical methods with low energy electron diffraction (LEED). It is shown that by use of this combination of techniques the enthalpy and entropy of adsorption onto well-ordered surfaces can be determined directly. The effect of imperfections in the surface on adsorption enthalpy can be readily determined using stepped surfaces (i.e. ordered periodic imperfections). The variation of enthalpy and entropy with coverage on structurally homogeneous surfaces can provide insight into substrate-adsorbate and adsorbate-adsorbate interactions.

2. Thermodynamics of Electrodeposition

The deposition of a ionized species from solution onto a metal electrode surface may, without loss of generality, be considered to proceed via an intermediate state, usually termed the "underpotential" state. We shall consider only underpotential deposition reactions which may be written as simple charge transfer steps

$$A^{Z+} + Ze^- \rightarrow A^* \qquad [1]$$

where A^* is the adsorbed (ad-atom) state on the electrode surface, and A^{Z+} is the solvated cation species. Implicit in equation [1] is the fact that there is a change in the solvation shell around A. The change in total entropy for the adsorption reaction will reflect this change in solvation and the magnitude of the $T\Delta S$ term to the total change in free energy is not insignificant. As the ad-atom concentration increases, association occurs leading to the formation of the bulk phase, as

$$(A^*-)A^* \rightarrow A_b \qquad [2]$$

The energetics of this association reaction may be used to define the thermodynamics of the underpotential state. We define the enthalpy change in [2] by ΔH^*,

$$\Delta H^* = -(2D_{AM} - D_{AA}) \qquad [3]$$

where D_{AM} is the dissociation energy of A^* from the metal substrate and D_{AA} is the dissociation energy of A from A. For an energetically homogeneous surface, and assuming no interactions between ad-atoms, we can define an isotherm for A^* based on the magnitude of $\Delta G^* \equiv \Delta H^* - T\Delta S^*$

$$\frac{\theta}{1-\theta} = a_A^{1/2} \exp(-\Delta G^*/2RT) \qquad [4]$$

where a_A is the thermodynamic activity of the bulk phase A. In an electrochemical cell at equilibrium, the thermodynamic activity of the bulk phase is related to the electrode potential via the Nernst relation

$$E = E_o - \frac{RT}{2ZF} \ln (a_A / a_A{}^{Z+}) \qquad [5]$$

where E is the potential of the electrode (at which deposition of A is occurring) relative to any reference electrode and E_o is the potential of the electrode when A is at unit activity (relative to the same reference electrode). It is convenient to define the electrode potentials only in terms of $U \equiv E-E_o$, i.e. against an A/A^{Z+} reference electrode in the same solution, so that

$$U = - \frac{RT}{2ZF} \ln a_A \qquad [6]$$

or

$$a_A^{1/2} = \exp(- ZFU/RT)$$

Finally we define the ideal relation between the coverage of the substrate surface by ad-atoms and the electrochemical potential in terms of the standard free energy of adsorption

$$\frac{\theta}{1-\theta} = \exp(-\Delta G_o^*/2RT) \exp(- ZFU/RT) \qquad [7]$$

The standard free energy of absorption, ΔG_o^*, is consequently $2ZFU_{1/2}$, where $U_{1/2}$ is the potential when $\theta = 1/2$.

Isotherms recorded at variable temperature may be used to calculate isoteric heats of adsorption (W) by use of the relation

$$\left(\frac{d \ln a_A}{dT} \right)_\theta = \frac{W}{RT^2} \qquad [8]$$

The entropy of adsorption can be obtained as a function of coverage from the relation between $RT \ln a_A$ and W, i.e.

$$\Delta S^* = -\left(\frac{W}{T}\right) - R \ln a_A \equiv -\left(\frac{W}{T}\right) + \frac{2ZFU}{T} \qquad [9]$$

The great virtue of electrochemistry is that the relation between coverage and chemical potential can be measured directly and with great accuracy (10^{-3} ML). Experimentally, it is more convenient to measure the derivative of θ directly, then integrate to obtain θ. This is done by the method of linear sweep voltammetry. When the potential of an electrode is changed, current flows in the external circuit which is the sum of two contributions, one representing the (dis) charging of the electrical double-layer, another the (dis) charging of the adsorbate layer, e.g.

$$i = dq/dt \qquad [10]$$

$$= \left(\frac{dq^{ads}}{dU}\right)\left(\frac{dU}{dt}\right) + C_{d\ell}\left(\frac{dU}{dt}\right) \qquad [11]$$

Then

$$aQ\left(\frac{d\theta}{dU}\right) = (i - aC_{d\ell})$$

$$\left(\frac{d\theta}{dU}\right) = (i/aQ - C_{d\ell}/Q) \qquad [12]$$

where a ≡ sweep rate and Q is the charge required to form a monolayer of adsorbed species. The double-layer capacitance, $C_{d\ell}$, of the high work function metals that one normally uses as electrode substrates (e.g. Pt, Au, Hg, etc.) are typically 10- 40 $\mu F/cm^2$, depending on the electrolyte. Since Q ≡ 200- 300 $\mu C/cm^2$, the double-layer (dis) charging contribution to [12] is therefore typically 0.05 -$0.1V^{-1}$ independent of sweep rate. The relationship between the experiment, which measures i vs. U during a linear sweep, and the derived isotherm is shown graphically in Fig. 1. Isotherms can be obtained from linear sweep voltammetry in the manner described only if the system is perturbed under reversible conditions, i.e. the coverage at a given potential

is independent of the sweep rate. The criterion of reversibility is easily verified experimentally, and in some cases it cannot be met at any (practical) sweep rate, as is the case for the underpotential deposition of oxygen on Pt group metals. The shape of the i - U curve contains information about the nature of the adsorbate interactions. This is illustrated in Fig. 1b using the simplest model for interactions, one in which the isoteric heat of adsorption changes linearly with coverage. For repulsive interactions ($g > o$), the peak maximum moves to lower potential and the peak shape is much broader than ideal. For attractive interactions ($g < o$), the peak maximum moves to higher potential and the peak shape is narrower than ideal. More complex and physically more realistic models of adsorbate interaction, such as dipole-dipole or image dipole interactions, have been calculated by Conway and co-workers (3) and show qualitatively the same behavior as in Fig. 1b but with asymmetric peak shapes. Therefore, i - U curves from structurally homogeneous surfaces (single crystals) provide at least a qualitative indication of the nature of the non-ideality of the absorption reaction and the relative importance of adsorbate interactions. Further detail on these interactions can best be derived by analysis of the variation in the isoteric heat of adsorption and differential entropy of adsorption with coverage.

Some confusion frequently occurs when thermodynamic quantities derived from electrochemical measurements are compared to what may be the comparable thermodynamic quantity derived in a non-electrochemical (i.e. no electrolyte) measurement. As defined here, the thermodynamic functions ΔG^*, ΔH^* and ΔS^* all refer to the same reference state, the bulk phase at unit activity. What we measure electrochemically is the change in state variable between that reference state and the underpotential state (submonolayer ad-atoms on a substrate in solution). The non-electrochemical experiment, e.g. vacuum deposition, has the same reference state and has a similar, but not identical, final state. The difference in thermodynamic quantities measured by the two methods reflects a difference in the chemical state of the ad-atoms in the two environments and not a difference in the manner of measurement per se. We shall be discussing, in a later section, detailed comparisons of thermodynamic functions determined with and without a solution phase.

3. Experimental Methods

The basic principle of ex-situ analytical methods is to couple electrochemical cells to UHV chambers where the plethora of techniques for the study of the vacuum interface can be used to examine the electrode surface. The directness of this coupling varies from laboratory to laboratory, from very crude (pull the electrode from the cell, carry it two buildings away, and insert into a UHV system) to very sophisticated (direct transfer with differential pumping). Depending on the particular system under study and the type of analysis being done ex-situ, crudely coupled systems suffice, e.g. RHEED analysis of metal electrodeposits (4). Glove-box transfer appears to be adequate for the study of the "near-surface" region, e.g. RHEED and XPS type analysis. However, for definitive work on

submonolayer species, the highest standards of UHV practice must be applied to the transfer of the electrode surface to and from the analytical chamber.

The experimental apparatus as used in our laboratory for the study of the underpotential states of hydrogen and oxygen on Pt is shown in Fig. 2. The single crystals were spot-welded to gold wires and suspended from a stainless steel block. The block was transferred from the manipulator in the LEED-AES bell-jar to the electrochemical cell by means of two polished stainless steel rods; vacuum sealing of the rods was accomplished using Viton O-rings radially compressed. The working electrode compartment, and the high-vacuum parts of the system, were isolated from the electrolyte reservoir and reference electrode via a glass-break. The transfer system and working electrode compartment were differentially pumped to about 1.3×10^{-6} Pa (1×10^{-8} Torr) after a bakeout at 423 K. In the typical experiment, a new single-crystal was mounted on the transfer block and attached to the vertical motion transfer rod with the electrochemical cell detached. The transfer block was transferred to the horizontal motion rod, the electrochemical cell attached to the system, and the entire transfer system pumped out to 2×10^{-6} Pa. The single crystal was then transferred to the ultra-high vacuum system, where it was cleaned by simultaneous argon ion bombardment and electron beam heating to 973 K. The ultra-high vacuum system was fitted with a rotary-motion feed-thru with a threaded tip with which the transfer block could be picked up and rotated, permitting ion bombardment and LEED/AES analysis to be carried out on both sides of the crystal. LEED analysis was accomplished using conventional 4-grid optics (Varian) and Auger analysis used a single pass CMA with 3 keV integral electron gun (Varian). The Auger spectrometer system also had sample imaging capability so that the entire surface of the crystal was analyzed for

impurities. The structure of the surface was then determined using LEED. After structure analysis was performed, the crystal was transferred into the working electrode compartment and the electrochemical system was isolated from the LEED-AES system by closure of the straight-thru valve. The working electrode compartment was then backfilled with Research Grade argon (Airco, 5 N purity) to near ambient pressure, and the electrolyte introduced by breaking the glass seal.

Since the cell configuration employed here required complete submersion of the crystal, regions of the crystal that are not well-ordered are contacted by electrolyte and thus contribute to the voltammogram, e.g. the edge. Typically the geometric area of edges on these crystals was 20% of the area of the polished faces, and the effective area even greater because of roughness. The contribution of the crystal edges to the voltammogram was measured directly by a gold masking technique. After obtaining the voltammogram for the complete crystal, gold was evaporated onto the polished faces so that just the edges and near-edge region of the Pt crystal were exposed to electrolyte. The voltammogram for these disordered regions was obtained following the same procedure as used for the crystal without the gold mask. To facilitate data manipulation the voltammograms were digitized and recorded in a multi-channel analyzer. At least two other electrochemical research groups have employed systems of the type shown in Fig. 2 to study underpotential states on single crystal electrode surfaces (5,6). However, the apparatus at our laboratory is the only system of its type in which variable temperature in the electrochemical cell is easily accomplished. The problem with this system is that the volume of electrolyte is quite large and it is difficult to purify the solutions to the extent necessary. The thin-layer cell employed by the Yeager group (6) appears to solve this electrolyte purity problem by increasing the surface to volume ratio by three orders of magnitude.

4. Underpotential States of Hydrogen on Pt

If two Pt foils are suspended in water (containing sufficient salt to provide conductivity) and maintained at a potential difference > 1.23 V, hydrogen will be evolved from the negative electrode and oxygen from the positive. If we measure the current passed during a linear sweep of the voltage (relative to a third reference electrode) of either electrode, we find that current is passed at potentials well below the thermodynamic potential difference. These currents correspond to the adsorption of water dissociation products that are intermediates in the formation of hydrogen and oxygen. Formally, these adsorbed species are referred to as the underpotential states of hydrogen and oxygen. Figure 3 shows linear sweep voltammetry curves for a clean, annealed, polycrystalline Pt foil in dilute sulfuric acid electrolyte obtained in the apparatus of Fig. 2. The reference electrode was a reversible hydrogen electrode in the same electrolyte with hydrogen at unit activity (101.3 k Pa pressure). Therefore, the electrode potential scale of Fig. 3 is exactly U of equation [6], and sweeping the potential corresponds to sweeping the equivalent partial pressure of hydrogen, given by the relation

$$P_{H_2}^{1/2} = \exp(- FU/RT) \qquad [13]$$

The first sweep was cathodic, starting at 0.4V, and the cathodic current measured between 0.4 and OV corresponds to the adsorption (underpotential deposition) of hydrogen ad-atoms from solvated protons in solution.

$$[H_9O_4]^+ + M(e^-) \rightarrow MH + 4H_2O \qquad [14]$$

Because of the excellent kinetics of the recombination/dissociation reaction on Pt, the equilibrium concentration of molecular hydrogen is established near the electrode surface (the diffusion boundary layer).

$$2\ MH \rightleftharpoons H_2 \qquad [15]$$

The mirror image anodic currents observed on reversal of the linear sweep corresponds to the reaction [14] and [15] driven in the opposite direction. The sharply increasing cathodic current below 0.05V corresponds to the evolution of sufficient molecular hydrogen to achieve equilibrium partial pressures that approach 101.3 k Pa.

The anodic current measured at 0.8 - 1.3 V in Fig. 3 corresponds to the adsorption of intermediates in the formation of molecular oxygen from water, i.e. the underpotential states of oxygen. We shall discuss the underpotential states of oxygen separately in a later section of this lecture.

There are, clearly, multiple states of hydrogen adsorbed on Pt electrode surfaces, and the challenge to electrochemists in recent years has been to produce a definitive explanation of the multiplicity of these states. The use of ex-situ methods of surface analysis and systems like that in Fig. 2 have proven to be extremely useful. LEED has been used to provide definitive determination of the surface structure of Pt electrodes before and after contact with electrolyte; Auger electron spectroscopy used to monitor surface contamination and/or oxidation; UHV practice was used to assure no contamination of the surface occurred before or after contact with electrolyte. It has now been clearly demonstrated (7 - 10) that the multiplicity of states represents adsorption of hydrogen at sites of different geometric configuration, i.e. local ordered domains of different geometry. We shall review here some selected results from these studies.

4.1 Isotherms for Hydrogen on (111) and (100) Pt

Voltammetry curves for hydrogen adsorption-disorption on (111) and (100) Pt single crystal electrodes are shown in Figs. 4 & 5. In both cases, post-test LEED analysis indicated the surfaces were the (1 X 1) structures during the experiment. In the case of the (100) crystal, the results in Fig. 5 were

obtained with an oxygen treated crystal in which the oxygen was left on the surface, so that the starting surface was (1 X 1)-O. Yeager's group (11) has reported that a different result is obtained if one uses the clean (5 X 20) reconstructed surface of the (100) crystal, and that transformation to the (1 X 1) surface occurs commensurate with hydrogen chemisorption. When the curves in Figs. 4 & 5 were corrected for edge effects using the gold masking technique described, the result was a single asymmetric peak for each surface. Isotherms for those single states, derived by integration of the corrected i - U curve, are shown in Fig. 6. The isotherms are clearly non-Langmuirian. The iso steric heat of adsorption on both surfaces falls monotonically with coverage (Fig. 7). It seems unlikely that progressive filling of sites of different energy would produce a monotonic function for the isosteric heat of adsorption. It seems more likely that the surface is energetically homogeneous and that adsorbate induced interactions caused the monotonic decrease in the heat of adsorption. The classical models of Roberts (12) for dissociative adsorption on identical sites with nearest neighbor interaction can be applied directly to compute the differential (isoteric) heat of adsorption. For a surface of uniform sites, the adsorption entropy for a diatomic molecule varies slowly with coverage for $\theta < 0.8$ (13), and for our purposes here we assume ΔS^* is essentially constant. Then

$$\Delta G^*(\theta) = - W(\theta) - T \Delta S_i^* \qquad [16]$$

where $W(\theta) \equiv - \Delta H^*$ is given by one of the models of adsorbate-adsorbate interaction. If the hydrogen ad-atoms are mobile at the temperature of adsorption, then (12)

$$W(\theta) = W_o - n\gamma \left(1 - \frac{1 - 2}{[1 - 4(1 - \rho)\theta(1 - \theta)^{1/2}}\right) \qquad [17]$$

where ρ is the Boltzmann factor $\exp(-\gamma/RT)$, W_o is the initial (zero coverage) heat of adsorption, and γ is the pair-wise interaction energy. For repulsive interaction, $\gamma > 0$ and the heat of adsorption decreases with coverage; for $|\gamma| < RT$, Taylor series of expansion of eq.(7) yields a linear change in the heat of adsorption $W(\theta) = W_o - n\gamma\theta$. Adsorption isotherms with a linear variation in adsorption free energy have been used extensively for the modeling of underpotential deposition (e.g. ref. 14) and it is well known that the linear function does not produce an asymmetric voltammetry curve. However, if the hydrogen adatoms are immobile, the resulting isotherm produces an asymmetric curve and a heat of adsorption function which fits the observed variation extremely well. For immobile adsorption (12),

$$W(\theta) - W_o - n\gamma \left[\frac{(n-1)^2}{n} \theta \frac{(2n-\theta)}{(n-\theta)} \right] \qquad [18]$$

The best values of W_o, the heat of adsorption at zero coverage, and γ were derived by fitting [7], [16], and [18] to the isotherms for the (111), $n = 6$, and the (100), $n = 4$, surfaces simultaneously, then checking the resulting $W(\theta)$ function against the experimentally observed variation. The best-fit values of ΔH_i^*, ΔS_i^*, and γ are given in Table 1, the calculated isotherms and the calculated $W(\theta)$ functions appear as the solid curves in Figs. 6 and 7, respectively.

Table 1. Thermodynamic functions[a] for the adsorption of hydrogen on Pt single crystal surfaces.

Surface	ΔH_i^* (kJ/mol)	ΔS_i^* (J/mol-K)	γ (kJ/mol-pair)
(111)	-46.8	-55.8	5.0
(100)	-81.1	-53.1	5.0

[a] Zero coverage at 300 K.

While the theoretical isotherms are not a perfect fit to the experimental curves, the asymmetry of the voltammetry curve for the (100) surface is predicted as well as the general form of the functional relation between isosteric heat of adsorption and coverage.

In principle, it should be possible to calculate the ΔS^* term for mobile and immobile dissociative adsorption and determine whether the values in Table 1 are consistent with the assumption of an immobile state. However, in the case of adsorption at surfaces in solution, the problem of solvent orientation makes this calculation less than straightforward. Figure 8 shows the classical electrochemical view (the BDM theory) of the water-hydronium ion double-layer (15) and a hypothetical view of the manner in which hydrogen adatoms are chemisorbed. The BDM double-layer model was developed specifically for the mercury electrode, but should apply to any metal electrode where there is no specific (chemical) interaction between water and the metal surface. This model should, therefore, apply to a Pt electrode at potentials positive to that for hydrogen adsorption and negative to that for OH formation. The layer of water molecules, strongly oriented with the positive end of the water dipole towards the metal surface, must be displaced by the hydrogen ad-atoms. There has been no model developed to predict the relaxation of the double-layer following hydrogen chemisorption, so there is no firm physical basis for calculating the total change in entropy. Until a great deal more is known about the structure of the double-layer when adsorbed hydrogen is present on the surface, it is not possible to calculate the "expected" values for the entropy of adsorption.

4.2 Hydrogen at stepped surfaces

As Somorjai and co-workers have shown (16), certain high Miller index faces of fcc metals form terraced surface structures with monoatomic steps. Cutting a (111) Pt rod at a progressively increasing angle along the zone line

between the [111] and [110] pole produces a series of (111) terrace structures, denoted [n(111) X (111)] in the notation of Lang and Somorjai (17). The clean, annealed surface of (110) Pt in vacuo has a (2 X 1) reconstructed surface. Ducros and Merrill (31) proposed a "sawtooth" structure consisting of tilted (111) microfacets for the (110) - (2 X 1) surface. Ball models of the sawtooth structure (Fig. 9) indicate the "trough" in this structure has the same site coordination as along the steps on [n(111) X (111)] surfaces, and can really be regarded as a vicinal of the [n(111) X (111)] group. It would be expected, therefore, that comparison of underpotential hydrogen on (111), [7(111) X (111)], [4(111) X (111)], and (110) would reveal the effect of adsorption at the four-fold sites (designated C^4_{110}) that exist at the steps in the [n(111) X (111)] surfaces and in the "trough" of the (110) - (2 X 1) surface. The ratio of four-fold step sites (C^4_{110}) to three-fold hollow sites (C^3_{111}) on the terraces varied in this series from 0, to 1:6, to 1:3 and to 1:1, respectively. The voltammetry curves shown in Fig. 10 clearly delineate a second peak (at 0.225V) whose peak area ratio to the primary peak was about the 1:3 and 1:1 expected if the secondary peak does represent adsorption at C^4_{110} sites and the primary peak adsorption at C^3_{111} sites.

Just as crystals produced by cutting a (111) rod at sequentially increasing angles toward the [110] pole revealed adsorption at sites having the (110) surface geometry, cutting a (111) rod at progressively increasing angles towards the [110] pole revealed adsorption at sites characteristic of (100) geometries. Figure 11 shows a series of voltammetry curves for a [n(111) X (100)] family of surface structures produced by cutting a (111) rod at selected angles towards the [100] pole. If we assume that adsorption at the steps occurs at the four-fold sites of (100) geometry (C^4_{110}) and at the terraces in the three-fold sites of (111) geometry (C^3_{111}), then the ratio of step sites to terrace sites on the crystals (111) would be 0, 1:6, 1:3, and 1:2 respectively. States

associated with the steps are clearly delineated in the voltammograms of Fig. 11, and the total charge associated with the steps was about that expected if only half the C^3_{111} sites are filled, as was the case for the ordered (111) crystal. However, unlike the (111) steps, two states of hydrogen are associated with adsorption at (100) steps, one state being more strongly bound at the (100) step than at the macroscopic (100) surface. It is not clear at this time what these two states correspond to, i.e. what site geometries are associated with each state.

Voltammetry curves taken at variable temperature have indicated the heat of adsorption for the hydrogen adsorbed at steps is larger than for hydrogen adsorbed at <u>either</u> low index face (111) or (100). This observation is particularly interesting for the C^4_{110} site as the standard free energy of adsorption at these sites is intermediate between that for the low index faces, meaning that the entropy of adsorption at C^4_{110} sites is significantly more negative than the value reported in Table 1. Qualitatively, more negative adsorption entropy implies more restricted motion of the adsorbate, i.e. less mobile. Again, however, the problem of coupled reorganization of the double-layer makes rigorous association of the total entropy change to the adsorbate alone inpossible. Nonetheless, it can be said that the sum of the adsorbate contribution and the double-layer contribution to the total entropy change indicates that the final state (hydrogen adatoms plus water dipole layer) is more ordered at monoatomic steps than at low index surfaces.

5. Underpotential States of Oxygen on Pt

In the linear sweep voltammetry curve of Fig. 3, the anodic currents observed in the potential region >0.7V correspond to what may be termed thermodynamically as the underpotential states of oxygen. Figure 12 shows this region in greater detail, with the anodic limit of the potential scan increasing. The criterion for reversibility of a surface faradaic process is that the anodic and cathodic wave-forms not be displaced from each other in potential (18). Reversibility is required if we are to extract the thermodynamic functions via the underpotential. For underpotential oxygen on Pt, the potential region of reversibility is quite restricted, as the cathodic peaks in Figure 12 start to lag the anodic peaks at potentials above 0.82V. Above 0.82V, the anodic surface species becomes progressively more irreversible. There have been a very substantial number of studies conducted over the years to identify the molecular species corresponding to the "reversible" and "irreversible" states, but definitive identification has been elusive. The present interpretation has changed little since the 1973 paper of Conway and co-workers (19). We shall use their interpretation in this discussion, and further restrict the discussion to the behavior of the surface in acid solution only. The initial portion of the anodic wave corresponds to dissociation of H_2O to form chemisorbed OH,

$$H_2O + M \rightarrow MOH + H_9O_4^+ + 1e^- \qquad [19]$$

The reversible OH species is the only species present up to ca. 25% of a monolayer (1 ML is 210 $\mu C/cm^2$ on a polycrystalline electrode). As the coverage is increased beyond 0.25 ML, the surface is reconstructed via

the place exchange mechanism shown in Figure 13. LEED studies in our laboratory tend to support this reconstruction hypothesis (19). Diffraction patterns were observed after cycling a Pt (111) surface to varying anodic potentials. As shown in Figure 14, the angular width of the (01) spots in the LEED increased when the anodic potential was increased above 0.8V, which is just the potential where reconstruction starts to occur. The reconstruction process may also be viewed as an "oxide" underpotential process. Pt atoms which have undergone place exchange have largely OH nearest neighbors, as is the case for Pt atoms in the hydrated oxide, $Pt(OH)_2$. The standard potential for formation of the bulk hydrated oxide $Pt(OH)_2$, via

$$Pt + 2H_2O \rightarrow Pt(OH)_2 + 2\ H_9O_4^+ + 2e^- \qquad [20]$$

is 0.98V (20). Figure 12 shows clearly that the irreversible OH species forms at a potential "under" the standard potential for the hydrated oxide.

The irreversibility of the $\frac{1}{2}\ O_2/H_2O$ reaction means we cannot define a thermodynamic underpotential scale equivalent to RT ℓn P, as we did in the case of the H_2/H_2O reaction. What the voltammetry curve of Figure 12 tells us is that reaction [19] is kinetically dominant in the potential region below 0.98V, and the reversibility of the reaction makes it possible to define an underpotential scale equivalent to RT ℓn a_{OH}. Then the state variables ΔH^* and ΔS^* for the formation of surface OH can be measured in the same manner as used for hydrogen. The results are summarized in Table 2. The reference state for these functions corresponds to the dissociated state of OH at unit activity, i.e. the equilibrium

$$H_2 + O_2 \rightleftharpoons 2(OH)_{ads} \qquad [21]$$

As with hydrogen, the adsorbed state of OH refers to a surface submerged in aqueous solution, so that the electrochemical adsorption process would include a term for the reorganization of the double-layer. In this case, however, the enthalpy is so large this reorganization term would contribute little to the total energy. We might expect therefore that the desorption energy of OH on Pt to the gas-phase as measured in a UHV apparatus and the adsorption enthalpy measured electrochemically would be reasonably close. This point will be discussed further in a later section.

The transition in the structure of the OH layer on Pt at potentials well below the potential for oxygen evolution has a profound consequence on the kinetics. At potentials close to the theoretical potential for O_2 evolution; i.e. RT ℓn $P_{O_2} \rightarrow 0$, the coverage of the surface by OH species exceeds 1 ML. If unoccupied Pt sites are required to catalyze the dissociation of H_2O to O_2, then the number of active sites available for O_2 evolution becomes exceedingly small.

Table 2. Thermodynamic Functions[a)] for OH Formation on Pt Single Crystal Surfaces.

Surface	H_i^* (kJ/mol)	S_i^* (J/mol K)
(111)	- 209.9	- 110.8
(110)	- 226.7	- 108.5

a) Zero coverage at 300 K.

The self-poisoning nature of this reaction illustrates one of the oldest concepts in heterogeneous catalysis, Sabatier's principle, that the intermediate must be adsorbed neither too weekly nor too strongly. So-called volcano relations, which are an expression of Sabatier's principle, between the enthalpy of formation of $M(OH)_n$ and the kinetics of oxygen evolution have been demonstrated by Appleby (21). All of the transition metals bond OH species even more strongly than Pt ($-\Delta H^* > 200$ kJ/mol OH), but the noble metals Ag and Au bond OH very weakly ($-\Delta H^* < 30$ kJ/mol OH). There is, therefore, a very large gap in adsorption energy between Pt and Ag or Au where one might expect to find the "optimum" catalytic surface, the surface more active for O_2 evolution (or oxygen reduction to water) than pure O_2. Phenomenologically, it is clear what properties the "optimal" electrode surface should have, i.e. weaker interaction with H_2O than Pt, stronger interaction with O_2 than Pt. There is, of cource, no material known which has these properties. One approach towards developing such materials is to look at modifications to the intrinsic properties of Pt by various means, e.g. doping, alloying, etc. There is some indication in preliminary work from our laboratory (22) that doping Pt with Group lVb and Vb elements produces a catalytically favorable modification to the intrinsic properties of pure Pt. More rigorous studies on the modified state of Pt in these alloys is in progress using UPS and XPS.

6. Underpotential States of Metals on Metals

Metal adsorbates on foreign metal surfaces are both fundamentally interesting and technologically important species. Technologically, they represent the initial stage for metal deposition and their structure should

influence the further growth behavior and final morphology of the deposit. Also, metal adatoms are believed to have electronic properties which are substantially different from those of the bulk metal and appear to have attractive catalytic properties (23). Fundamentally, metal adatoms are ideal systems for the study of lateral interactions between adsorbates and of phase formation on surfaces.

The underpotential deposition of metals on foreign metal electrode substrates is a widely studied phenomenon in electrochemistry, and the standard electrochemical methods of coulometry and linear sweep voltammetry provide means of directly measuring heat of adsorption, entropies of adsorption and, in most cases, absolute coverage. Absolute coverage can be accurately measured in any system if an independent method exists for determining the electrosorption valency. Ex-situ determination of the valency by XPS appears possible. The marriage of classical electrochemical methods with the ex-situ UHV methods of electron spectroscopy and electron diffraction should enable these metal-on-metal adsorbate systems to be studied in extraordinary detail. What makes ex-situ UHV analysis particularly attractive in this case is the generally high stability of the metal adatom layer which enables it to survive the vacuum transfer intact (24). The stability of these systems arises principally from the non-volatile and relatively immobile state of the adatom on the substrate surface. In spite of the particular attractiveness of ex-situ UHV analysis in these systems, there are no completed studies of underpotential metal deposition to report at this time, although a number are in progress. The research group of Kolb and co-workers at the Fritz-Haber Institute have, however, made detailed studies of metal adsorbates at both the

metal-vacuum and metal-solution interface and concluded that the presence of the solution had little or no effect on the structure of the adsorbate, i.e. the studies yielded complimentary information. It is of interest then to review the results for a system that appeared to behave "ideally" in that sense, Pb deposition on Ag(111). The electrolytic deposition of Pb was studied (24) in a conventional electrochemical cell in perchlorate solution using linear sweep voltammetry. Vacuum deposition was by electron beam evaporation, and LEED-AES-work function analyses were conducted on the deposited layer in a conventional (Varian) UHV chamber. Auger signal intensities of Pb and Ag indicated a sharp break at exactly the point where 1 ML of closely packed Pb atoms would be expected, indicating deposition starts in a layer-by-layer growth mechanism. In the submonolayer region, LEED analysis indicated the formation of two ordered structures (Fig. 15), a $(\sqrt{3} \times \sqrt{3})R\ 30°$ structure forming at $0.2 < \theta < 0.5$, and an hcp twist structure which coexists with the $(\sqrt{3} \times \sqrt{3})R\ 30°$ at $0.5 < \theta < 1.0$ ML and forms the overlayer structure at higher coverages. The LEED patterns correlated precisely with breaks in the $\Delta\phi$ vs. θ curves (Fig.16). Vacuum deposition of Pb on Ag(111), therefore, starts with the formation of a uniform monolayer in three steps: random adsorption followed by a $(\sqrt{3}X\sqrt{3})$ superstructure and lastly an hcp layer. Deposition of Pb from solution appears to follow <u>precisely</u> the same sequence, as indicated in the linear voltammetry curve of Fig. 17. There are two distinct transitions indicative of three deposition processes; the transitions occurred at 0.2 and 0.5 ML, as was the case for vacuum deposition. The sharpness of the peak at 0.15V underpotential indicates the adatoms have an attractive interaction while the broad tail to the peak representing

the last Pb adatoms to be deposited is indicative of repulsive interaction. These interaction effects are consistent with the LEED structures in Fig. 15, since second nearest neighbor interactions represent attractive forces, and nearest neighbor interactions repulsive. Can we then say that electrodeposition and vacuum deposition of Pb on Ag(111) result in the formation of identical structures? The picture seems tantalizingly consistent and complementary, yet the parallels could be coincidental. However, truly definitive experiments utilizing direct coupling of the electrochemical cell to the UHV chamber appear possible. If the electrodeposition process is stopped at ca 0.5 ML, the electrolyte evaporated from the surface, the crystal transferred to the UHV chamber, and the LEED-AES -work function analysis gives the expected result, then the evidence would indeed be conclusive.

7. Relation of the Underpotential State to the Chemisorbed State in Vacuum

At least two underpotential states of atoms studied in considerable detail appear to form bonding configurations with the substrate surface very like those formed in the absence of electrolyte, i.e. at the vacuum interface. These are hydrogen atoms on Pt surfaces in dilute perchloric or hydrofluoric acid solutions, and Pb atoms on Ag surfaces in dilute sodium perchlorate solutions. Considering the imposing experimental problems associated with definitive tests of this proposition, it seems reasonable to examine carefully the rational basis behind it. Since we are, in the present context, restricting our attention to just the thermodynamic functions ΔH^* and ΔS^* relating adatoms to the bulk phase (reaction [2]), the thermodynamic cycle presented in Fig. 18 provides a convenient and direct way of relating adsorption at the metal-vacuum interface to adsorption at the metal-

solution interface. In the case of the total enthalpy change, ΔH^*, the enthalpy changes for dehydration (L_M), adsorption (W_{AM}) and solution (S_{AM}) are all experimentally measurable quantities, particularly for the case where the solution is pure H_2O (infinite dilution). Then the enthalpy of formation of the underpotential state (ΔH^*) is related to the gas phase heat of adsorption (W_{AM}) by

$$-\Delta H^* = W_{AM} - (L_M - S_{AM}) \qquad [22]$$

If it takes more energy to remove H_2O from the bare metallic surface than is released when the adsorbate coverage surface is immersed, then $-\Delta H^*$ is less than the gas phase heat of adsorption, and vice versa. There are two sets of circumstances where it would be expected that $-\Delta H^* \simeq W_{AM}$. If the enthalpies of dehydration and immersion are essentially equal ($L_M \simeq S_{AM}$), or if the heat of adsorption in very large relative to either ($W_{AM} >> L_M$, S_{AM}), then the gas phase heat and the solution phase enthalpy should be equal. The thermodynamic cycle of Fig. 18 suggests a whole new avenue of experimental research for electrochemists who want to relate in a rigorous way the underpotential state to the comparable state in vacuum in order to understand electrode processes more fully. The key element in this new, non-traditional approach to the study of electrode processes is the study of water on all metallic surfaces of interest (as electrodes), with and without adatoms or adsorbed species of interest, using entirely UHV methods. In a way, one would be "doing electrochemistry" entirely in UHV. Strictly speaking, the surface processes observed would apply only to electrode processes at pH $\simeq$ 7 in an infinitely dilute electrolyte. Additional and experimentally more difficult work will have to be done to

determine the role of cations and anions in order to extend the results to real electrolytes.

Fortunately, there is already a significant and rapidly growing body of literature on the interaction between water and clean metal surfaces. The heat of desorption of H_2O from metallic Pt surfaces (L_M) has been measured (25) and is only slightly higher than the heat of sublimation (60 kJ/mol vs. 42 kJ/mol) indicating the specific interaction between H_2O and Pt is weak. Unfortunately the heat immersion of a hydrogen covered Pt surface has not been measured, nor has the heat of adsorption of H_2O on a hydrogen covered Pt surface been measured. The author attempted the latter experiment in the apparatus of Fig. 2, but the heating configuration of the sample holder resulted in a heating rate too low for thermal desorption experiments. The weak specific interaction of H_2O with the Pt surface implied in the results of Fisher and Gland (25) indicates that the presence of hydrogen on the Pt surface should have little effect on the energy released on hydration of the surface, i.e. $L_M \simeq S_{AM}$.

In the particular case of Pt electrodes in very dilute aqueous solutions, there is, therefore, a rational basis for the expectation that the adsorption energies in solution and in vacuum be the same. For hydrogen chemisorption on Pt, a comparison of the electrochemical results from our laboratory with the vacuum experiments reported in the literature indicates the two methods give comparable adsorption energies, although there is considerable variation in the energies for hydrogen on (111) Pt between investigators. The binding states of hydrogen on (111) Pt in vacuum has been studied in detail by Ertl and co-workers (26), McCabe and Schmidt (27), and Lu and Rye (28) using the thermal desorption

method. However, the latter two studies did not have LEED capability in their systems to determine in a rigorous way the structure of their single crystal surfaces. McCabe and Schmidt and Lu and Lye both reported an adsorption energy (zero coverage) of 73.2 kJ/mol for (111) Pt, while Ertl and co-workers found a much lower value, 41.2 kJ/mol. The Ertl group reported that the adsorption energy of hydrogen on (111) Pt was very sensitive to the annealing of the ion bombarded surface, and that adsorption energies as high as 70-80 kJ/mol were observed on "imperfect" (non-annealed) surfaces. However, surfaces that produced "perfect" (111)-(1X1) LEED patterns produced the lower adsorption energy of 41.2 kJ/mol. Since neither of the other investigator's systems utilized LEED analysis of their surfaces, it seems likely the higher adsorption energies reported in those studies is not representative of "perfect" (111)-(1X1) surfaces. The value of 41.2 kJ/mol from the Ertl group is very close to the electrochemically determined value of 46.8 kJ/mol. Less work has been reported for hydrogen on (100) Pt. Qualitatively, hydrogen bonding is stronger on the (100) plane, as reported by both Lu and Rye (28) and McCabe and Schmidt (27). Quantitatively, the latter report initial heats of adsorption of 102.5 and 115 kJ/mol for hydrogen on (100) Pt above room temperature, significantly higher than the electrochemically determined value of 81.1 kJ/mol. As before, the absence of LEED structure analysis in the work of McCabe and Schmidt raises questions as to the nature of the surface in their experiments. Nonetheless, their results clearly indicate that the relative adsorption energy of hydrogen on (100) Pt is higher than on (111) Pt by ca. 40 kJ/mol, which is what the electrochemically measured values indicated as well. Further qualitative

agreement between electrochemically measured bond energies and the thermal desorption bond energy is evident when the results for stepped Pt surfaces are compared. This is done in Fig. 19 using the thermal desorption work of Collins and Spicer (29) and the electrochemical results of Ross (8). Collins and Spicer deconvoluted their thermal desorption spectra into a "terrace" and "step" contribution, the step contribution always occurring at higher binding energy than the terrace contribution. At the step of (111) X (100) geometry, the coverage by hydrogen is just twice that at the step of (111) X (111) geometry. Both these observations are precisely what was observed electrochemically (refer to the detailed discussion given in Section 4.2). Unfortunately, Collins and Spicer did not report absolute binding energies for hydrogen on their surfaces, so a quantitative comparison is not possible. It would appear that at present it is not possible to make quantitative comparisons of adsorption energies of hydrogen on Pt determined by electrochemical methods with those determined using thermal desorption methods in UHV. There are, however, a precise set of experiments that would make rigorous quantitative comparison possible:

i.) electrochemical measurements of adsorption energies at infinite dilution (pH-7);

ii.) definitive measurement of the heat of dehydration of the metallic surface (L_M) and the heat of solution of the adsorbate covered surface;

iii.) definitive experiments to determine the thermodynamic heat of adsorption of hydrogen on well-ordered single crystal surfaces in UHV.

The thermodynamic cycle of Fig. 18 is also useful in interpreting the entropy of adsorption in solution, but adsorption entropy is not a

state function easily measured in UHV systems. By their very nature, UHV methods rely on irreversibility of the adsorption in order to measure coverage via a spectroscopic method, e.g. AES. Equilibrium isotherms are therefore rarely obtained in contemporary surface studies, and consequently adsorption entropies are infrequently reported. There are notable exceptions, represented by the lectures given in this symposium by Professors Fain and Menzel. The use of the Kelvin probe method for dynamic measurement of the change in work functions upon adsorption appears particularly promising, since one can then obtain coverages of the surface under reversible (equilibrium) conditions. Menzel reported equilibrium isobars for hydrogen and carbon monoxide on Ru (0001), from which the heat of adsorption and the differential entropy of adsorption were obtained as a function of coverage. More widespread use of this technique, when applicable, should lead to more complete determinations of the thermodynamic properties of surfaces. Ertl and co-workers have also made extensive use of the Kelvin probe method, particularly for the study of hydrogen on metals, but have reported (13) isobars and differential entropies only for hydrogen on Pd (100). For that system, at 370 K, the partial molar entropy of the adsorbed phase is perfectly described by the model for two-dimensional translation of a system of non-interacting particles (Volmer gas). Below 370 K, the adsorbed layer can be described by a localized model, consistent with LEED indications of ordered states below 270 K. This order - disorder phenomena at ca 300 K is typical of hydrogen on the transition metals, and it probably occurs on Pt as well. The electrochemically measured value for the differential entropy of adsorption at zero coverage (ΔS_i^*), given in Table 1, was - 55.8 J/mol-K.

The reference state is the gas at 100.3 k Pa and 298 K. If we completely ignore the possible effect of water (actually the double layer including solvated protons and anions), we can calculate the partial molar entropy of the adsorbed phase ($\bar{S}_i^*$) at low coverage from the relation

$$\bar{S}_i^* = \Delta S_i^* + \bar{S}_g$$

At 100.3 kPa 298 K, $\bar{S}_g$ = +130.5 J/mol K (30), so that $\bar{S}_i^*$ = +75.2 J/mol K. This value agrees well with the value for a two-dimensional gas at $\theta \simeq 0.1$ and 298 K, + 94.5 J/mol K, relative to the much lower (factor of two) value for the configurational entropy of a localized adsorbate + 36.6 J/mol K. The electrochemically measured value for the differential entropy of adsorption therefore appears to be consistent with the gas phase results indicative of a mobile hydrogen adatom state.

The observant reader will have noted that the conclusion that the hydrogen adatom layer on Pt is mobile at room temperature conflicts with the immobile adsorbate model used to interpret the isotherms (eq [18]). The reason for this conflict is not clear. The analysis of adsorption entropy above ignored the possible effect of reorganization of the double-layer, so the derived partial molar entropy of the adsorbed phase could be misleading. However, the general mobility of hydrogen on transition metals in vacuum suggests the mobile interpretation may be the correct one. In that case, the Roberts pair-wise repulsive interaction model does not explain the observed dependence of isosteric heat of adsorption on coverage, or the asymmetry of the isotherm.

Pt and Au are unique electrode materials in that the specific interaction of these surfaces with aqueous electrolytes is very weak and the adsorption of neutral molecules (or atoms) at the metal/solution interface is relatively undisturbed by the presence of electrolyte. The heat of adsorption of hydrogen on Pt electrodes is higher than on any other electrode surface, yet, in vacuum, there are many metal surfaces at which hydrogen is bound much more strongly than at Pt, e.g. W. Other metals adsorbing hydrogen have much stronger specific interaction with water, resulting in lower net heats of adsorption of hydrogen on these metals in aqueous solution. Although Au does not chemisorb many neutral molecules, e.g. H_2, CO, C_2H_4, etc., it is the ideal surface for studying the adatom states of metals with a minimum of interference from the electrolyte. However, aside from these two metals, there appear to be few other electrode surfaces at which adsorption occurs with a minimum interaction between the solvent and the adatom. The underpotential states of hydrogen on Pt are, therefore, untypical states for electrode processes, and, in general, thermodynamic functions derived from underpotential measurements will not be the same as those measured in vacuum.

Acknowledgments

This work was supported by the Assistant Secretary for Fossil Energy, Office of Coal Utilization and Extraction, Advanced Concepts Division of the U.S. DOE under contract number W-7405-ENG-48 through the Fuel Cell Projects Office, NASA Lewis Research Center, Cleveland, OH.

References

1. R. P. Van Duyne, "Surface Enhanced Raman Spectroscopy," to be published in Proceedings of the 1979 ISISS.

2. R. O. Ansell, T. Dickinson, A. F. Povey and P. M. A. Sherwood, J. Electroanal. Chem., 98, 69, 79 (1979) and references therein.

3. B. E. Conway and H. Augerstein-Kozlowska, J. Electroanal. Chem., 113, 63 (1980).

4. H. O. Beckman, H. Gerischer, D. M. Kolb, and G. Lempfuhl, Symp. Faraday Soc., 12, 51 (1978).

5. A. T. Hubbard, R. Ishikawa, and J. Katekaru, J. Electroanal. Chem, 86, 271 (1978); T. E. Felter and A. T. Hubbard, J. Electroanal. Chem., 100, 473 (1979).

6. P. Hagans, Ph.D. Thesis, Chemistry Dept., Case Western Reserve University, Cleveland, OH, 1980; also E. Yeager, Surf. Sci., 101, 1 (1980).

7. P. N. Ross, J. Electrochem. Soc., 126, 67 (1979).

8. P. N. Ross, Surf. Sci., 102, 463 (1981).

9. E. Yeager, W. O'Grady, M. Woo and P. Hagans, J. Electrochem. Soc., 125, 348 (1978).

10. K. Yamamoto, D. Kolb, R. Koetz, and G. Lempfuhl, J. Electroanal. Chem., 96, 233 (1975).

11. E. Yeager, J. Electrochem. Soc., 128, 168C (1981).

12. J. K. Roberts, "Some Problems in Adsorption," Cambridge Univ. Press, 1939, pp. 21-41.

13. R. J. Behm, K. Christmann and G. Ertl, Surf. Sci., 99, 320 (1980).

14. B. E. Conway, H. Augerstein-Koxlowska, and F. C. Ho, J. Vac. Sci. Technol., 14, 351 (1977).

15. J. O'M. Bockris, M. A. Devanathan and K. Muller, Proc. Roy. Soc. (London) A297 (1963).

16. D. W. Blakely and G. A. Somorjai, Surf. Sci., 413 (1977); M. A. Van Hove and G. A. Somorjai, Surf. Sci., 92, 489 (1980).

17. B. Lang, R. Joyner, and G. A. Somorjai, Surf., Sci., 30, 440, 454 (1972).

18. P. Stonehart, H. Augerstein-Kozlowska, and B. E. Conway, Proc. Roy. Soc. (London), A310, 541 (1969).

19. H. Augerstein-Kozlowska, B. E. Conway, and W. B. Sharp, J. Electroanal. Chem., 43, 9 (1973).

20. M. Pourbaix, "Atlas of Electrochemical Equilibria in Aqueous Solutions," Pergamon Press, 1966.

21. A. J. Appleby, Catal. Rev.-Sci. Eng., 4, 221 (1970).

22. P. N. Ross, EPRI Final Report EM-1553, September 1980.

23. D. M. Kolb, in: Advances in Electrochemistry and Electrochemical Engineering, Vol. 11, H. Gerischer and C. Tobias eds. (Wiley, NY, 1978) p. 125.

24. K. Takayanagi, D. Kolb, K. Kambe, and G. Lehmpfuhl, Surf. Sci., 100, 407 (1980).

25. G. B. Fisher and J. L. Gland, Surf. Sci., 94, 446 (1980).

26. K. Christmann and G. Ertl, Surf. Sci., 60, 365 (1976); K. Christmann, G. Ertl and T. Pignet, Surf. Sci., 54, 365 (1976).

27. R. McCabe and L. Schmidt in: Proc. 7th Intern. Vacuum Congr. and 3rd Intern. Conf. on Solid Surfaces (Vienna, 1977) p. 1201.

28. K. Lu and R. Rye, Surf. Sci., 45, 677 (1974).

29. D. Collins and W. Spicer, Surf. Sci., 69, 85 (1977).

30. Lange's Handbook of Chemistry, John A. Dean ed., Eleventh Edition, 1973.

31. R. Ducros and R. Merrill, Surf. Sci., 55, 227 (1977).

Figure Captions

Figure 1(a). The shape of the current-voltage curve ($i \equiv Qd\theta/dU$) for an adsorption process and the corresponding isotherm; (b) the change in shape of the current-voltage curve when the adsorption is not ideal (g=o); g > o repulsive interaction; g < o attractive interaction.

Figure 2. Schematic of the electrochemical-surface analysis apparatus: (1) O-ring feed-thrus; (2) transfer rods; (3a) and (3b) transfer block with crystal suspended from wires; (4) gate valve; (5) straight-thru valve; (6) reference electrode; (7) counter electrodes; (8) glass-break and Luggin capillary. From P. N. Ross, Jr., Surf. Sci., 102, 463 (1981) with permission.

Figure 3. Cyclic voltammetry of a clean, annealed polycrystalline Pt foil in 0.5M H_2SO_4 following transfer from the LEED/Auger chamber.50mV/s. From P. N. Ross, Jr., Surf. Sci., 102, 463 (1981) with permission.

Figure 4. Voltammetry curve for hydrogen adsorption-desorption on Pt(111) single crystal (———); specific contribution due to crystal edge (····); curve for adsorption on the well-ordered (111) face after correction for the edge effect. 0.05M $HClO_4$.50mV/s. From P. N. Ross, Jr., Surf. Sci., 102, 463 (1981) with permission.

Figure 5. Voltammetry curves for hydrogen adsorption-desorption on Pt(100) single crystal (———); specific contribution due to crystal edge (·····); curve for adsorption on the well-ordered (100) face after correction for the edge effect. 0.05M $HClO_4$.50mV/s. From P. N. Ross, Jr., Surf. Sci., 102, 463 (1981) with permission.

Figure 6. Isotherm for hydrogen on the well-ordered (a.) (111) and (b.) (100) Pt surface; measured (o); isotherms calculated from Langmuir model

(– – –) and Roberts' model for immobile adsorption with repulsive interaction (———).300 K.

Figure 7. Isosteric heats of adsorption of hydrogen on (111) and (100) surfaces of Pt in dilute $HClO_4$ solution. Curves shown were calculated from Roberts' model for immobile adsorption with repulsive interaction. From P. N. Ross, Jr., Surf. Sci., 102, 463 (1981) with permission.

Figure 8(a). Classical electrochemical view of the water-hydronium ion double layer with contact adsorption of the anion; dipole arrow points to hydrogen end of H_2O molecule; (b) hypothetical displacement of H_2O from the innermost layer upon chemisorption.

Figure 9. Ball models of (a) the (100)-(1 X 1) unreconstructed surface (right) and the reconstructed (110)-(2 X 1) surface (left); (b) the [4(111) X (111)] stepped surface. Small clear balls represent the four-fold adsorption sites denoted C^4_{110} in the text.

Figure 10. Voltammetry curves for hydrogen adsorption-desorption on n(111) X (111) stepped surfaces. 0.05M $HClO_4$.50mV/s.

Figure 11. Voltammetry curves for hydrogen adsorption-desorption on n(111) X (100) stepped surfaces. 0.05M $HClO_4$.50mV/s. From P. N. Ross, Jr. Surf. Sci. 102, 463 (1981)

Figure 12. Cyclic voltammetry of polycrystalline Pt in θ.1M HF solution; underpotential states of oxygen are observed between θ.8 - 1.23V.

Figure 13. Place exchange mechanism for reconstruction of the Pt surface during anodic film formation. From H. Angerstein-Kozlowska et al., J. Electroanal. Chem., 43, 9 (1973) with permission.

Figure 14. Loss of order in the (111) Pt surface during anodic film formation as observed by LEED.

Figure 15. Submonolayer structures of Pb on (111) Ag surfaces deduced from LEED patterns: (a.) ($\sqrt{3}$ X $\sqrt{3}$) R 30° structure; (b.) co-existing ($\sqrt{3}$ X $\sqrt{3}$) R 30° and hcp twist structures; (c.) the hcp twist structure. From K. Takayanagi et al., Surf. Sci., 100, 407 (1980).

Figure 16. Work function changes due to deposition of Pb on (111) Ag surfaces. 1 and 2 denote coverages where changes in LEED patterns were observed.

Figure 17. Cyclic voltammetry of Pb deposition on (111) Ag. The potential scale is the underpotential scale, i.e. V vs. Pb/Pb^{2+} electrode in the same electrolyte. 1 and 2 denote potentials where the coverages were 0.2 and 0.5 ML, respectively. From K. Takayanagi et al., Surf. Sci., 100, 407 (1980).

Figure 18. Thermodynamic cycle relating the gas-phase heat of adsorption (W_{AM}) to the solution phase enthalpy of adsorption (ΔH^*) measured electrochemically.

Figure 19. Comparison of spectra for hydrogen chemisorbed on (111) X (100) and (111) X (111) stepped Pt surfaces: by thermal desorption in vacuum, from D. Collins and W. Spicer, Surf. Sci., 64, 85 (1977); by potential sweep in solution, from P. N. Ross, Jr., Surf. Sci., 102, 463 (1981).

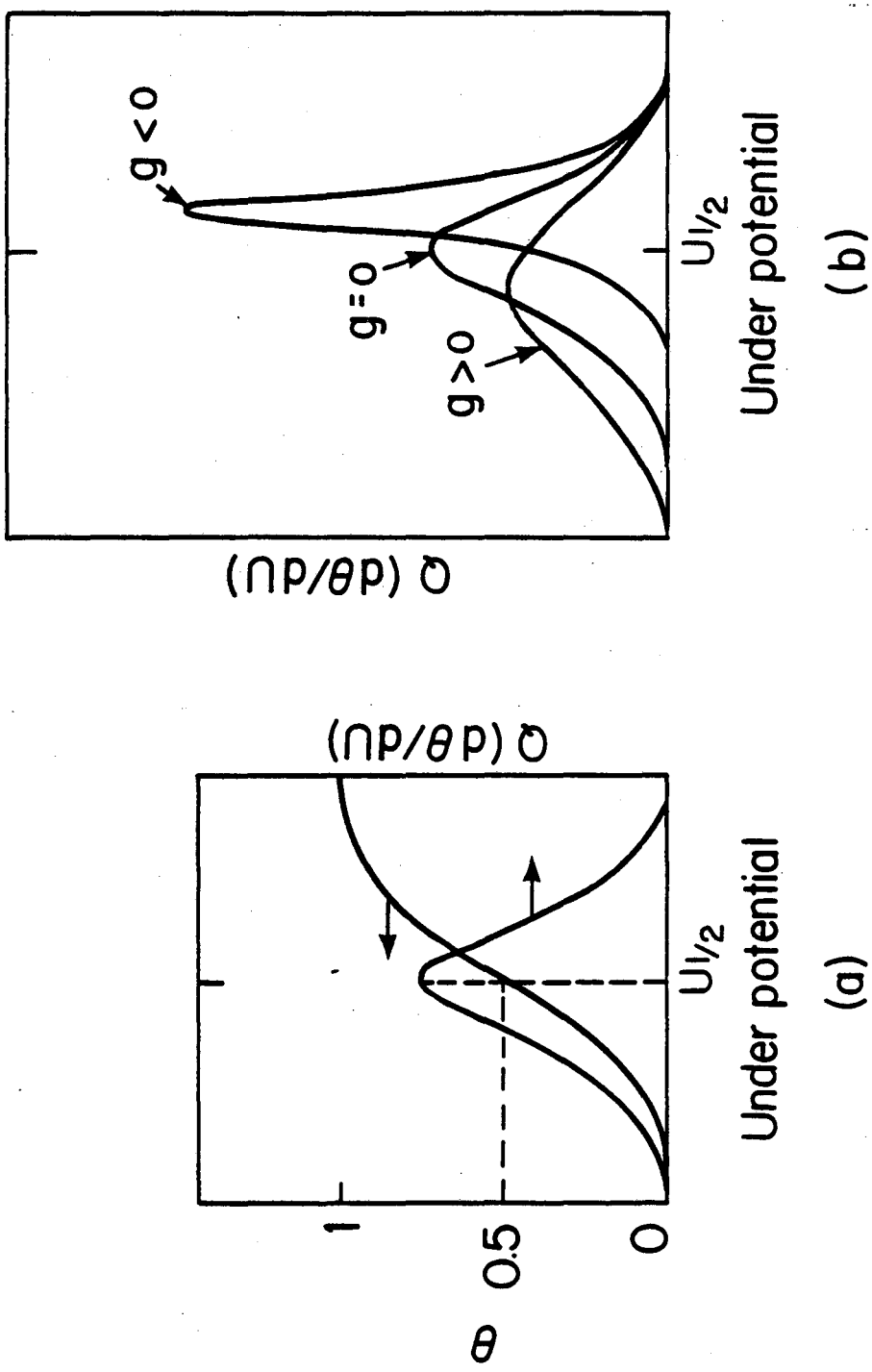

XBL 819-1349

Fig. 1

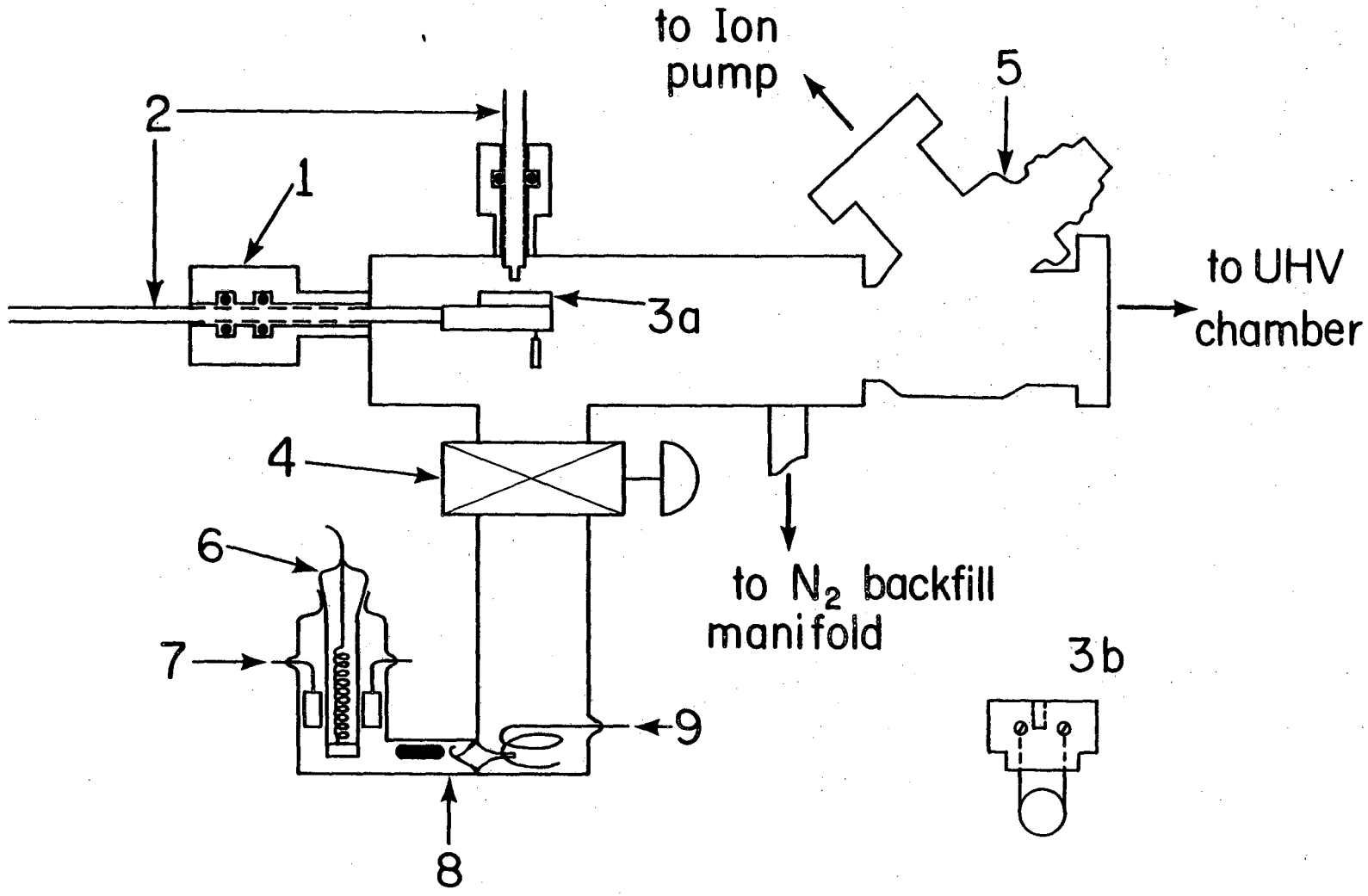

XBL 798-2475

Fig. 2

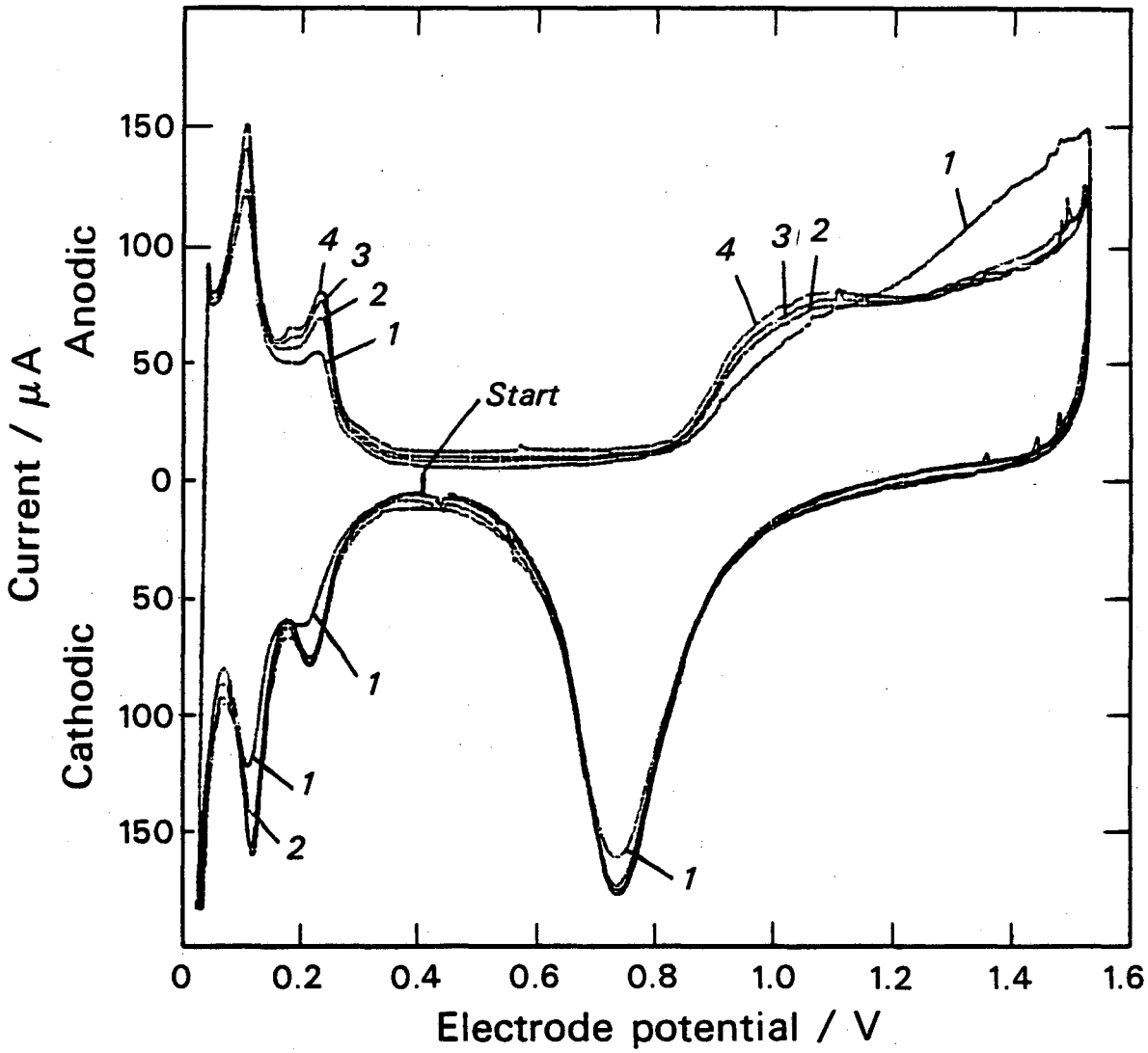
Current / μA
Anodic
Cathodic
150
100
50
0
50
100
150
0
0.2
0.4
0.6
0.8
1.0
1.2
1.4
1.6
Electrode potential / V
Start
1
2
3
4
XBL 804-666

Fig. 3

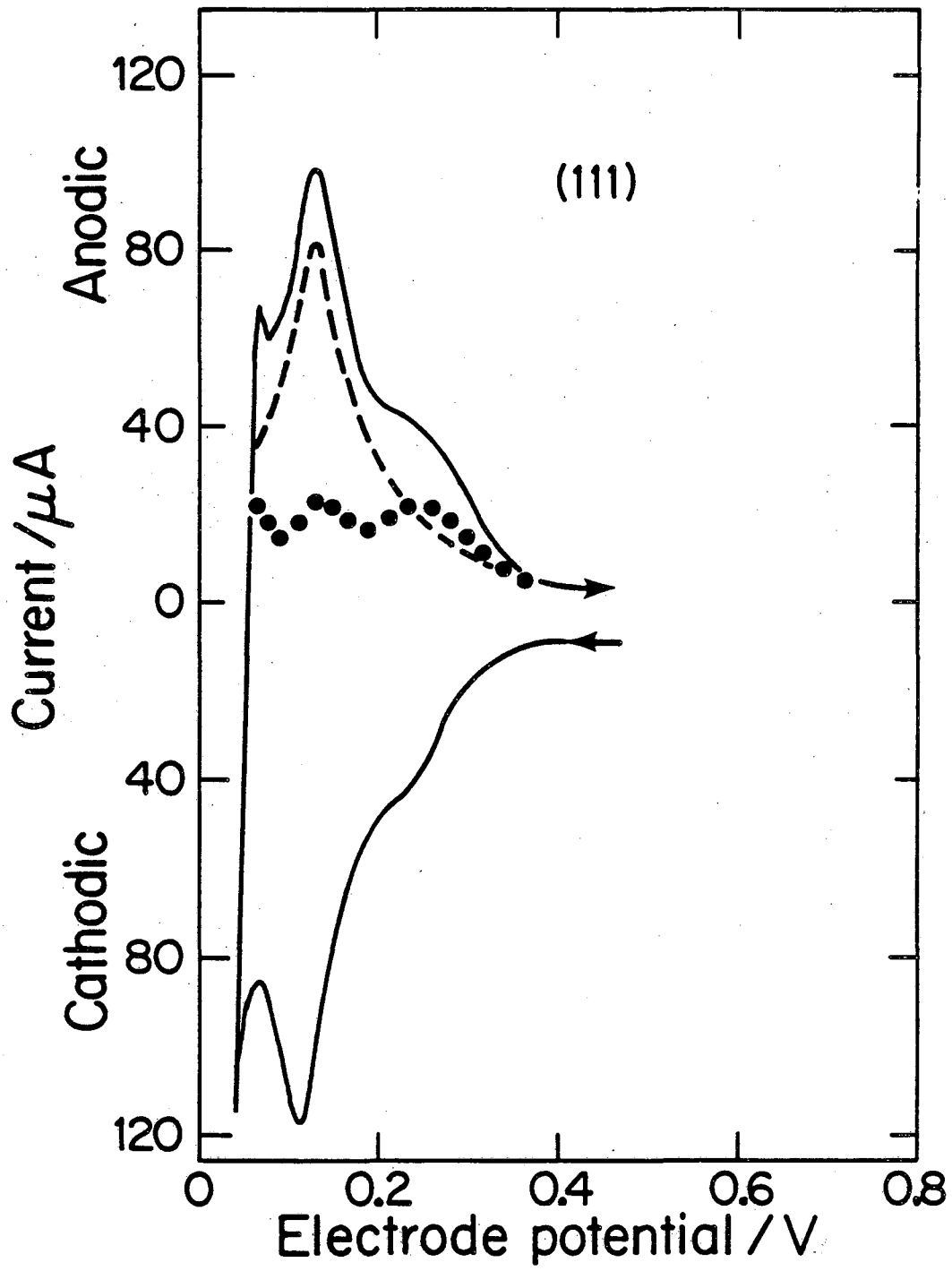

XBL 801 - 9

Fig. 4

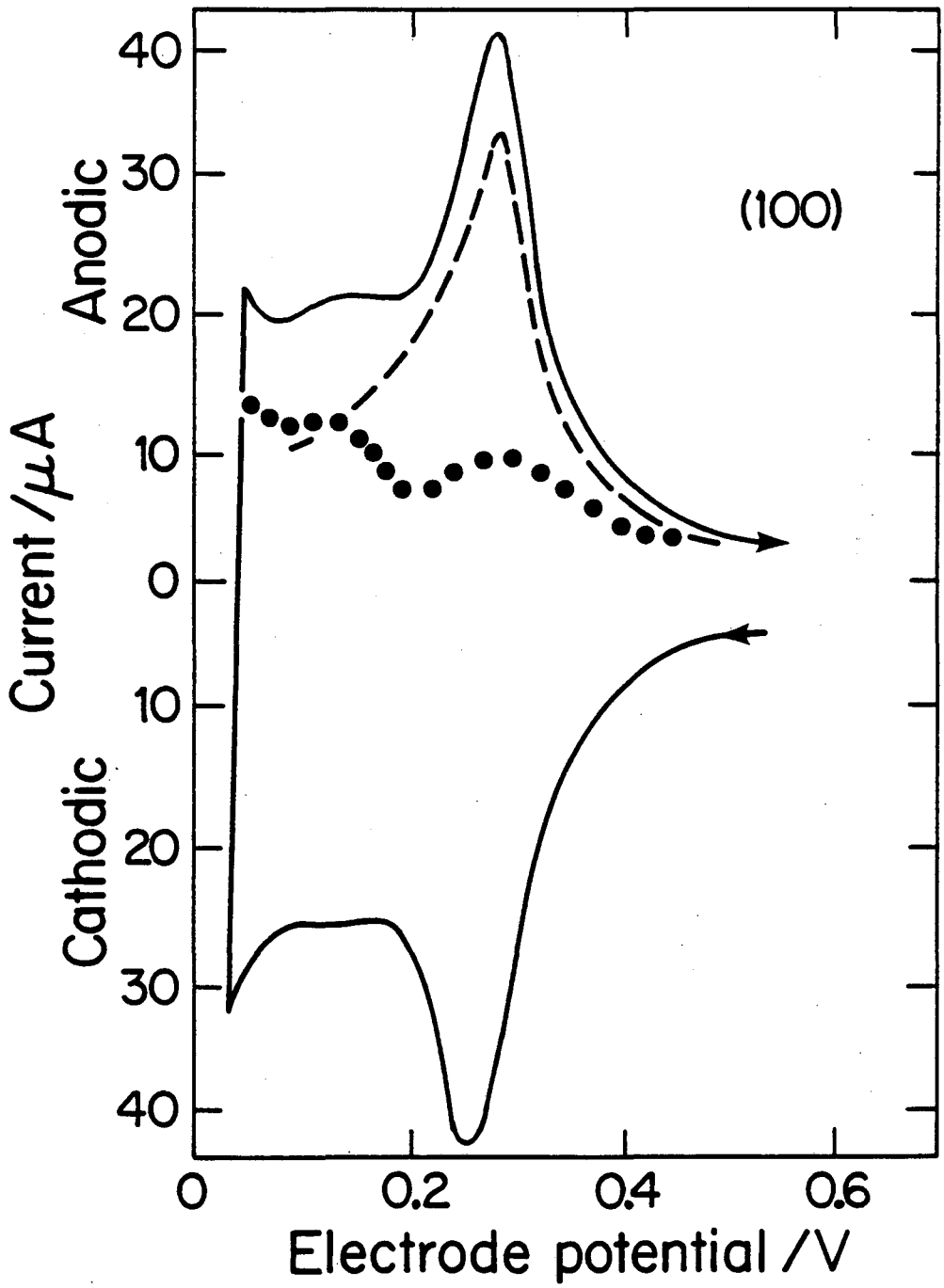

XBL 801 - 7

Fig. 5

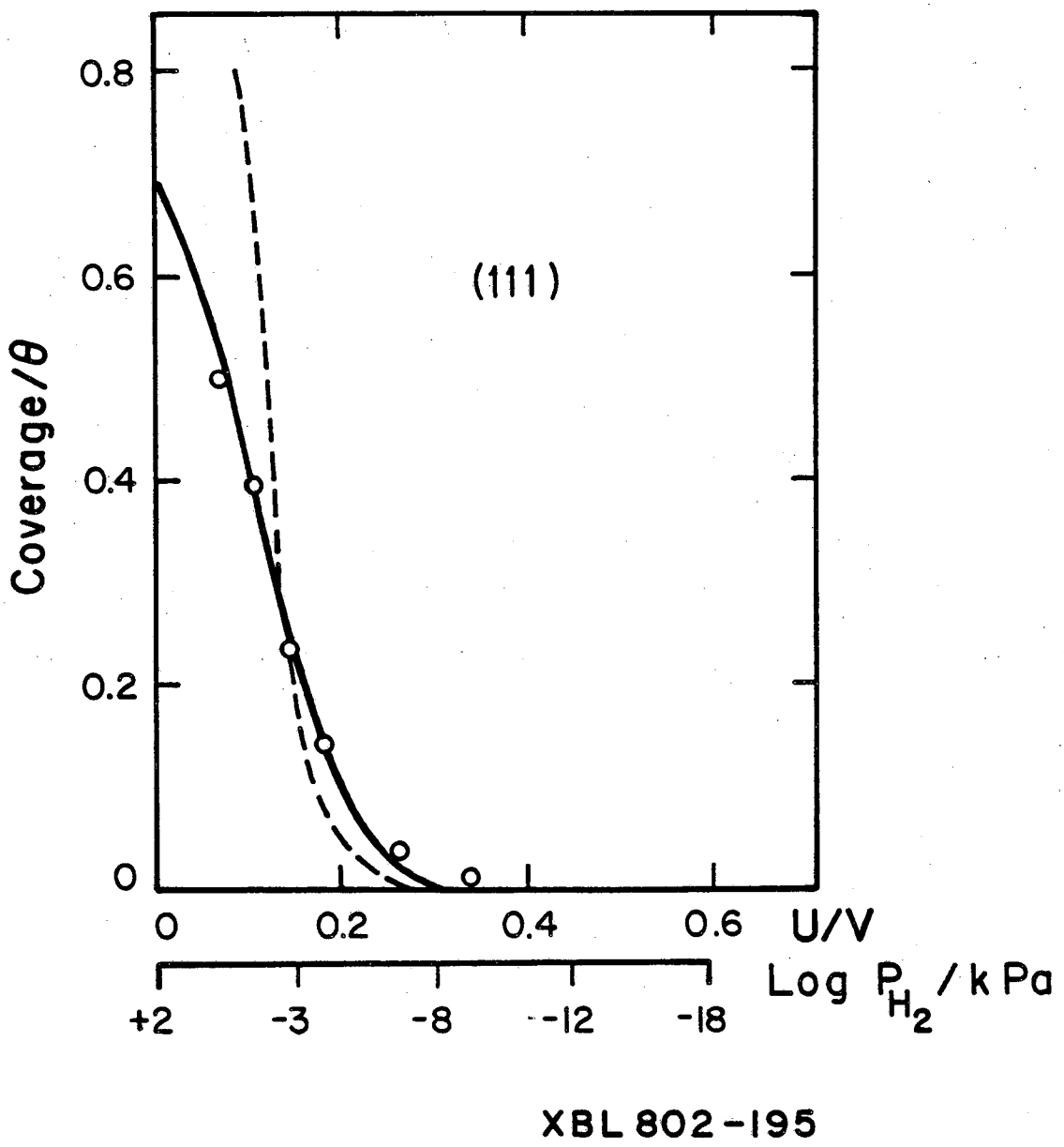
0.8
0.6
0.4
0.2
0
Coverage/θ
(111)
0
0.2
0.4
0.6
U/V
Log P_{H_2} / kPa
+2
-3
-8
-12
-18
XBL 802-195

Fig. 6(a.)

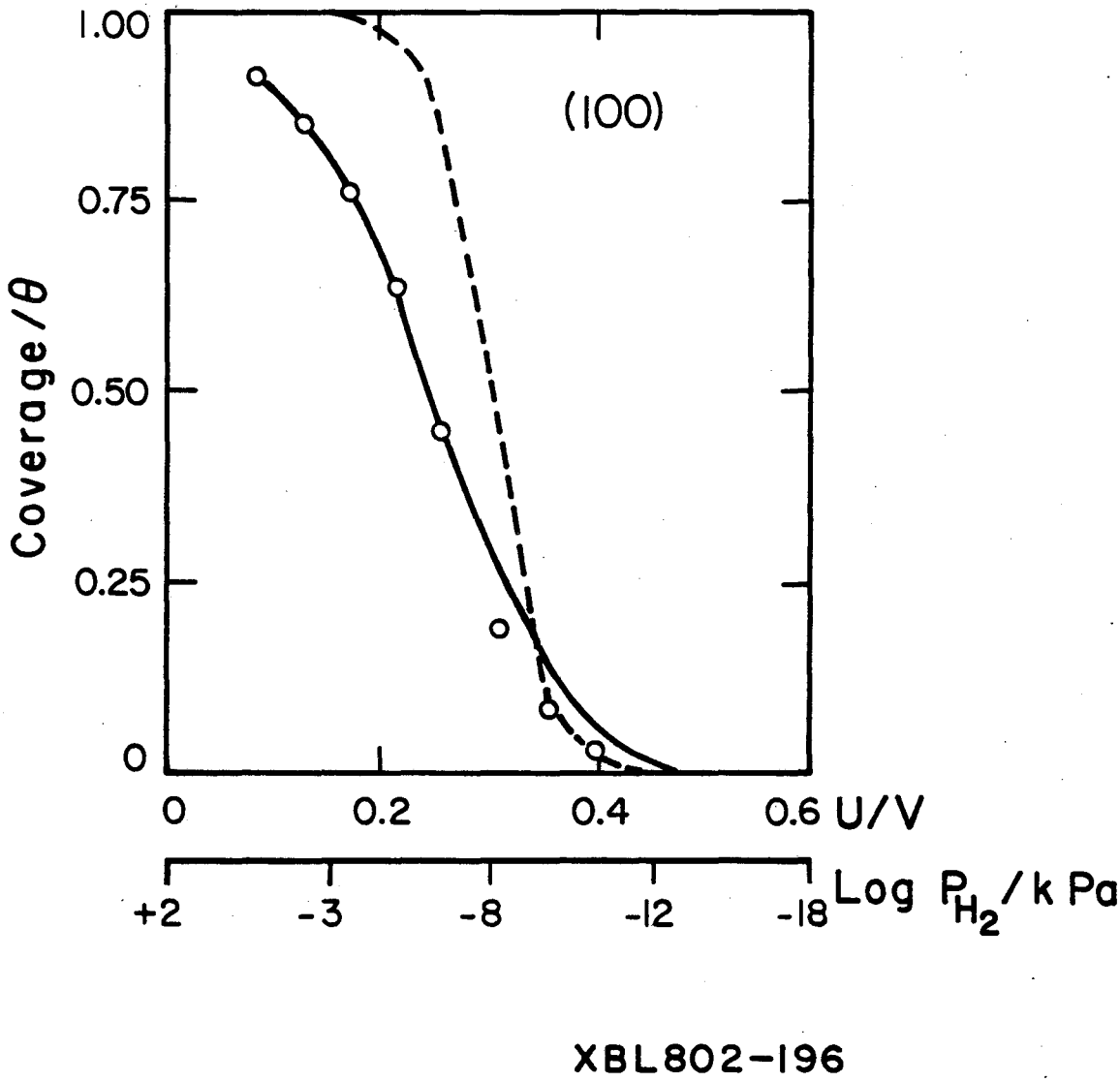
1.00
0.75
0.50
0.25
0
Coverage/θ
(100)
0
0.2
0.4
0.6 U/V
+2
-3
-8
-12
-18
Log P_{H_2}/k Pa
XBL802-196

Fig. 6(b.)

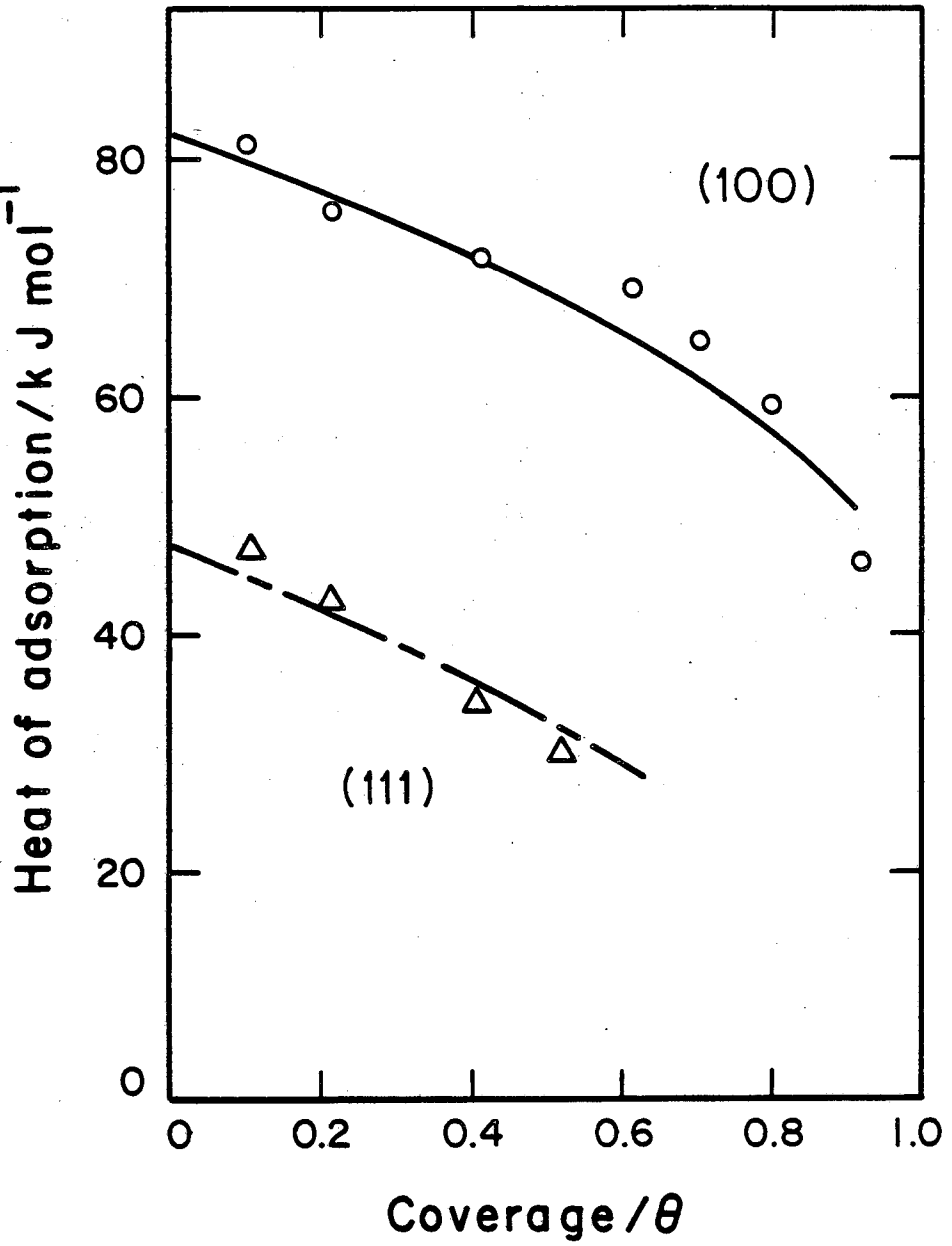

XBL802-199

Fig. 7

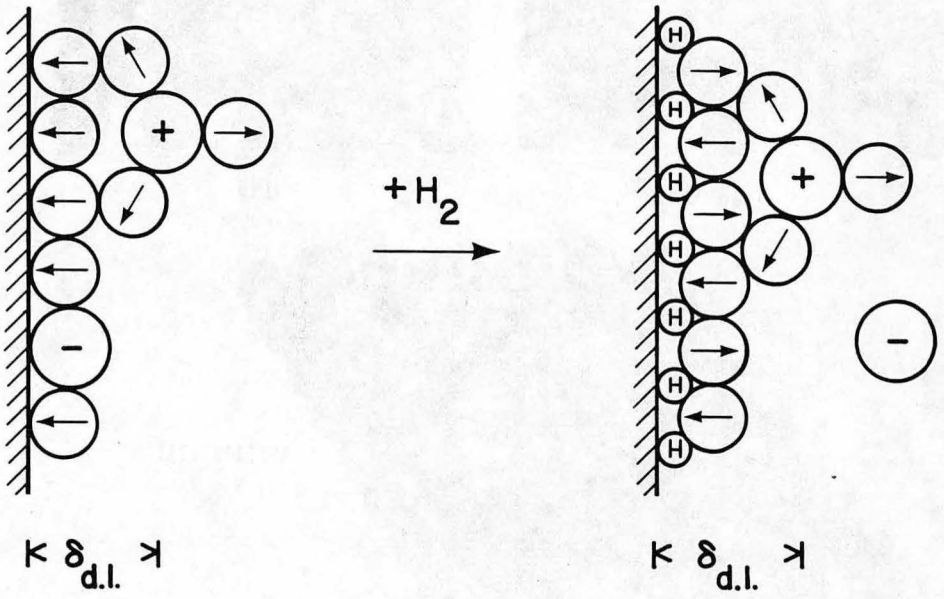

XBL 818-1221

Fig. 8

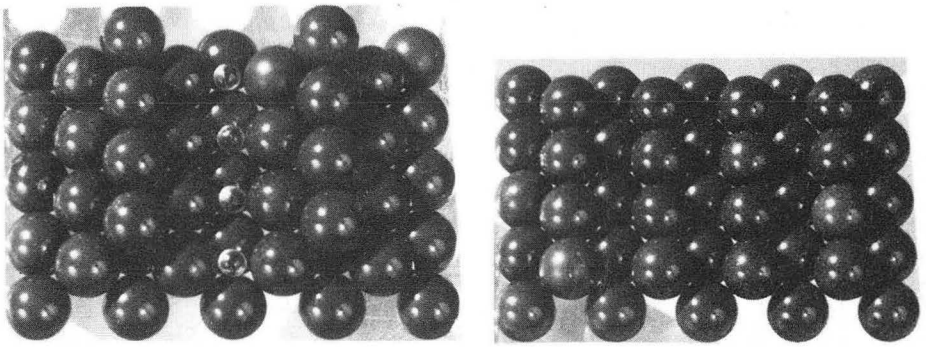

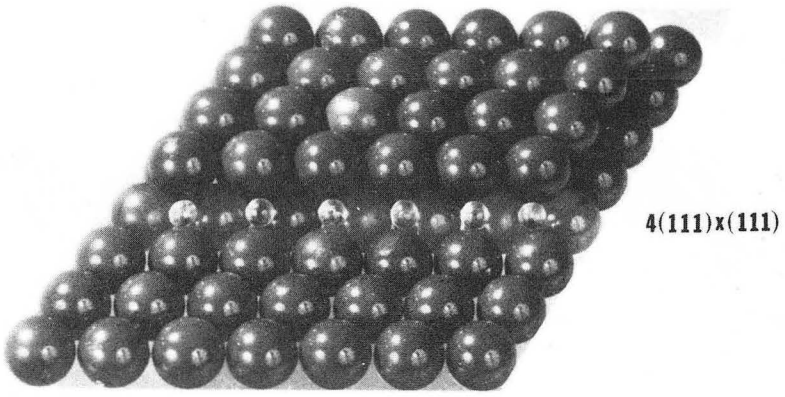

XBB804-4104

Fig. 9

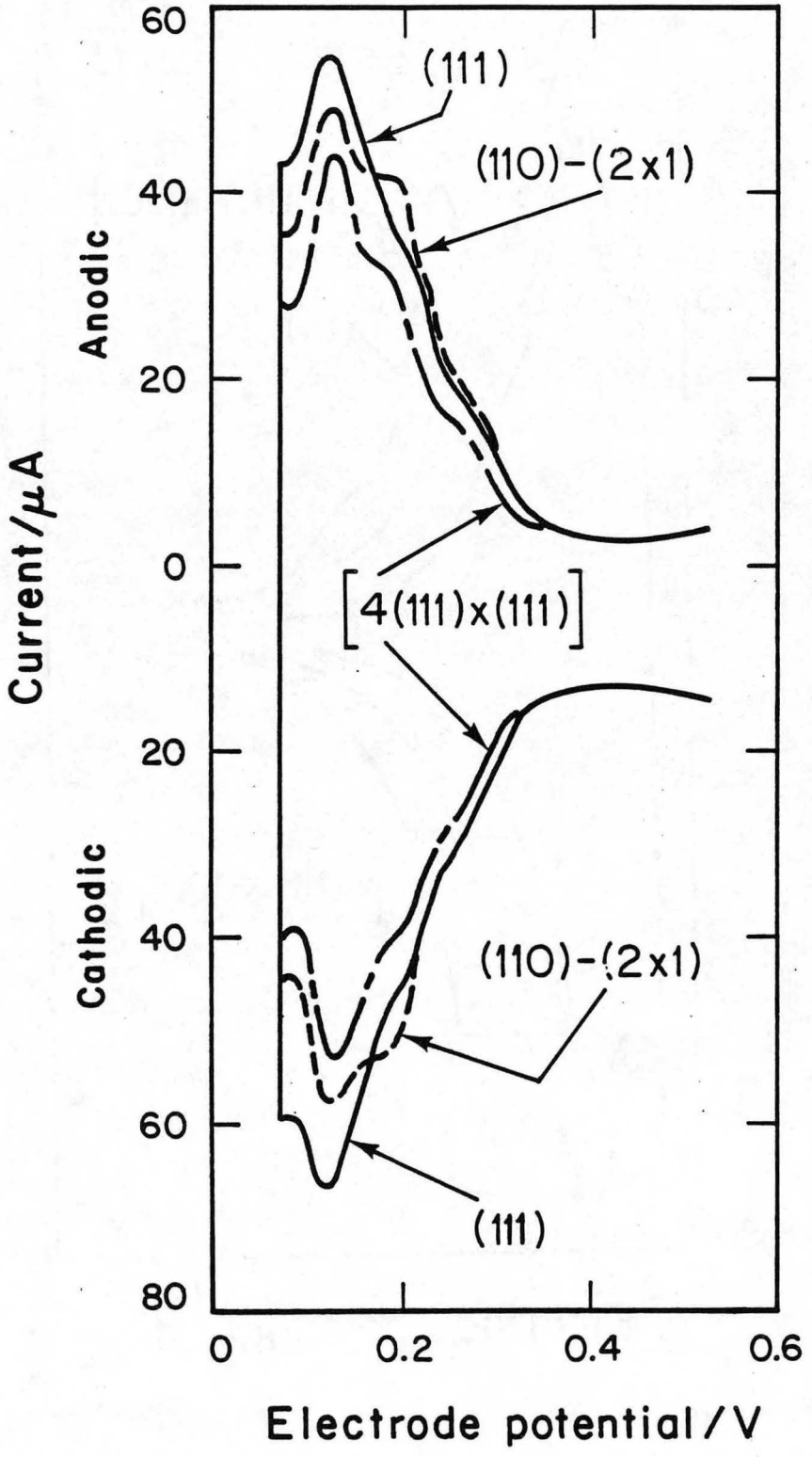

XBL 802-194

Fig. 10

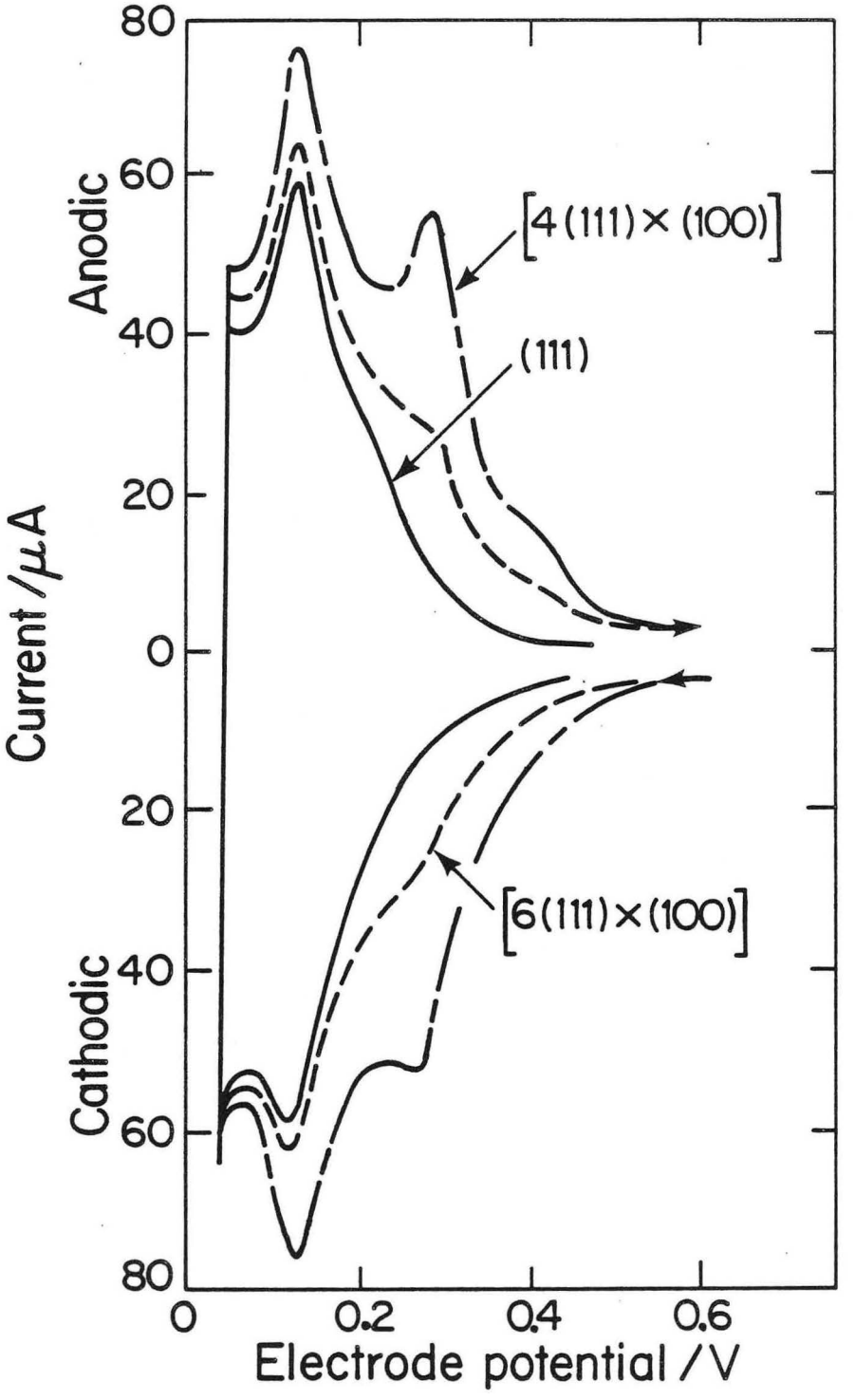

XBL 801 - 8

Fig. 11

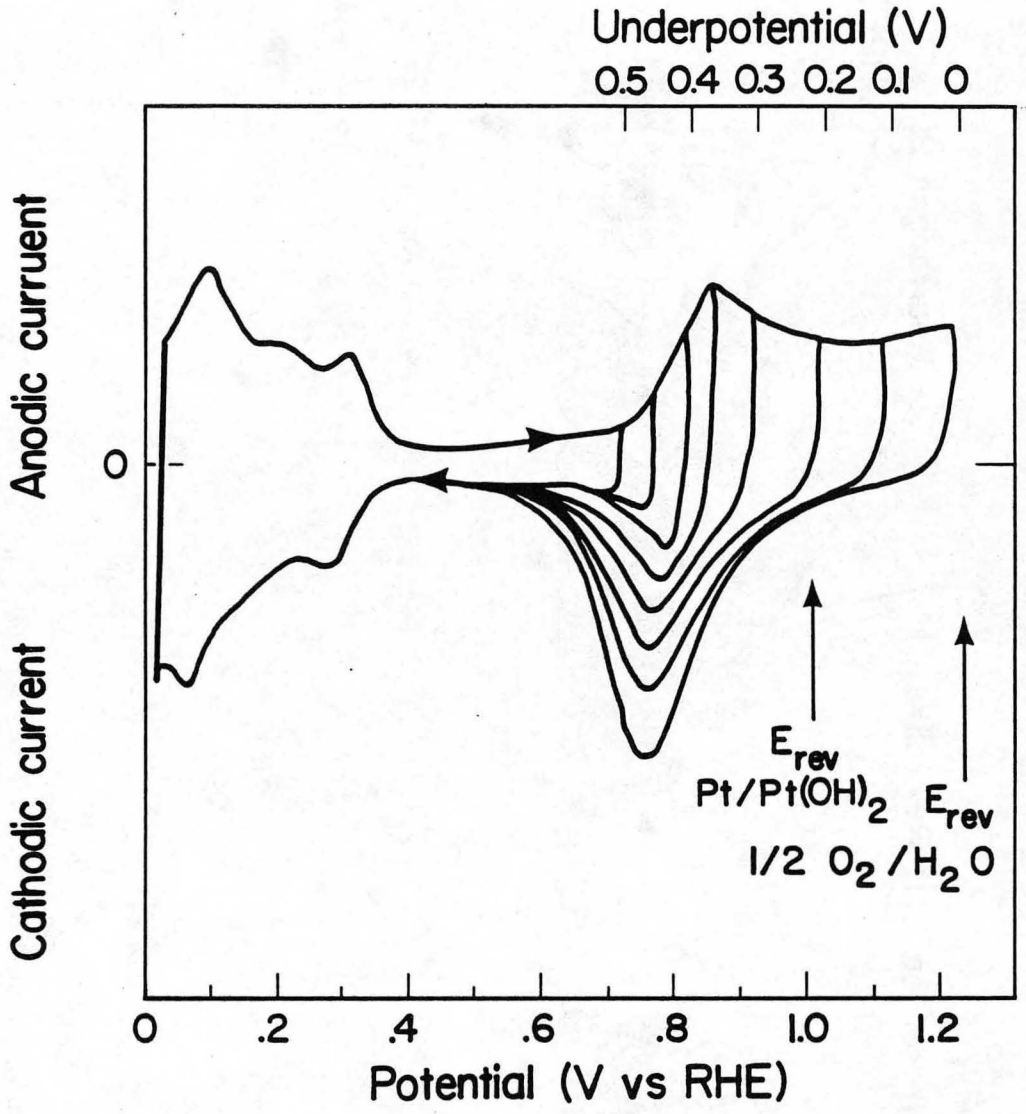

XBL 818-1223

Fig. 12

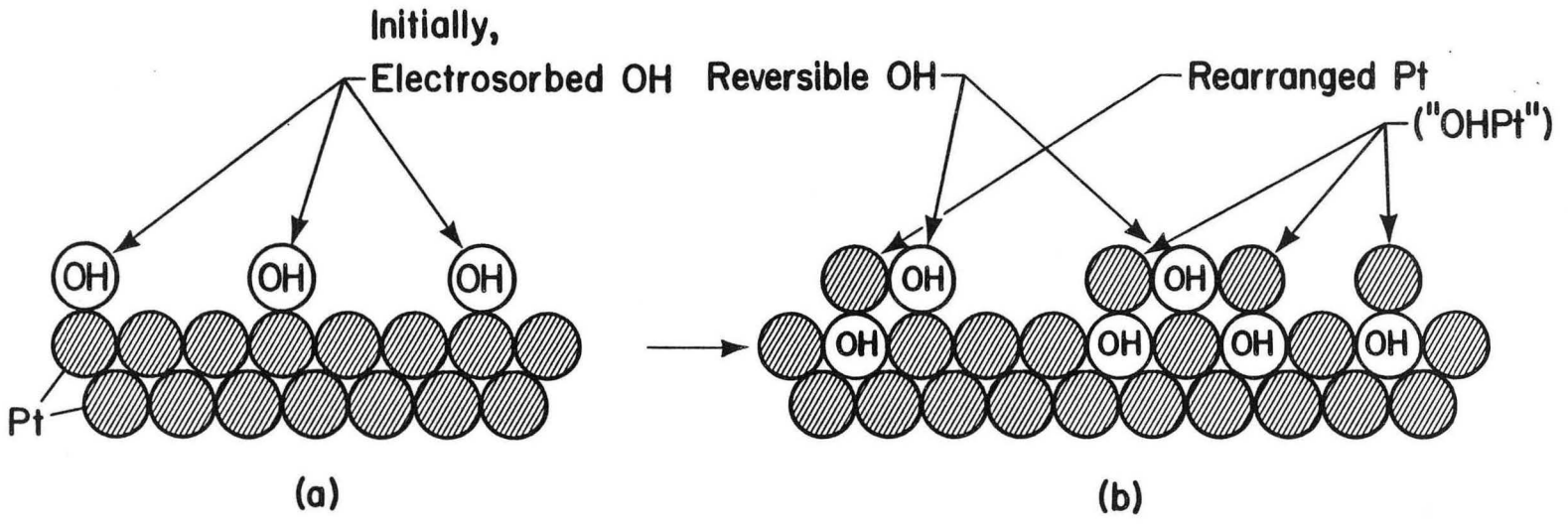
Initially,
Electrosorbed OH
Reversible OH
Rearranged Pt
("OHPt")
OH
Pt
(a)
(b)
XBL 818-1222

Fig. 13

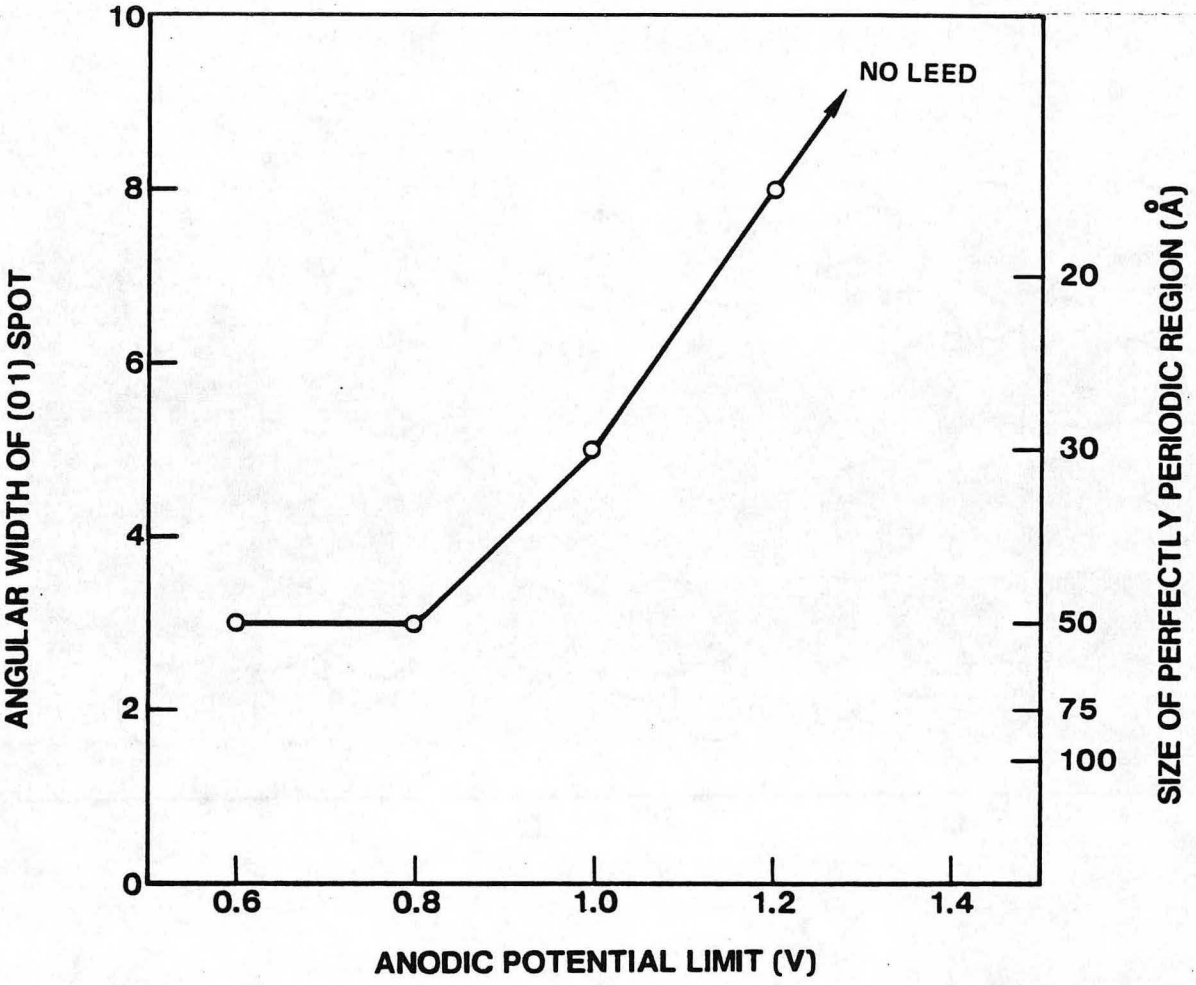

XBL 797-10619

Fig. 14

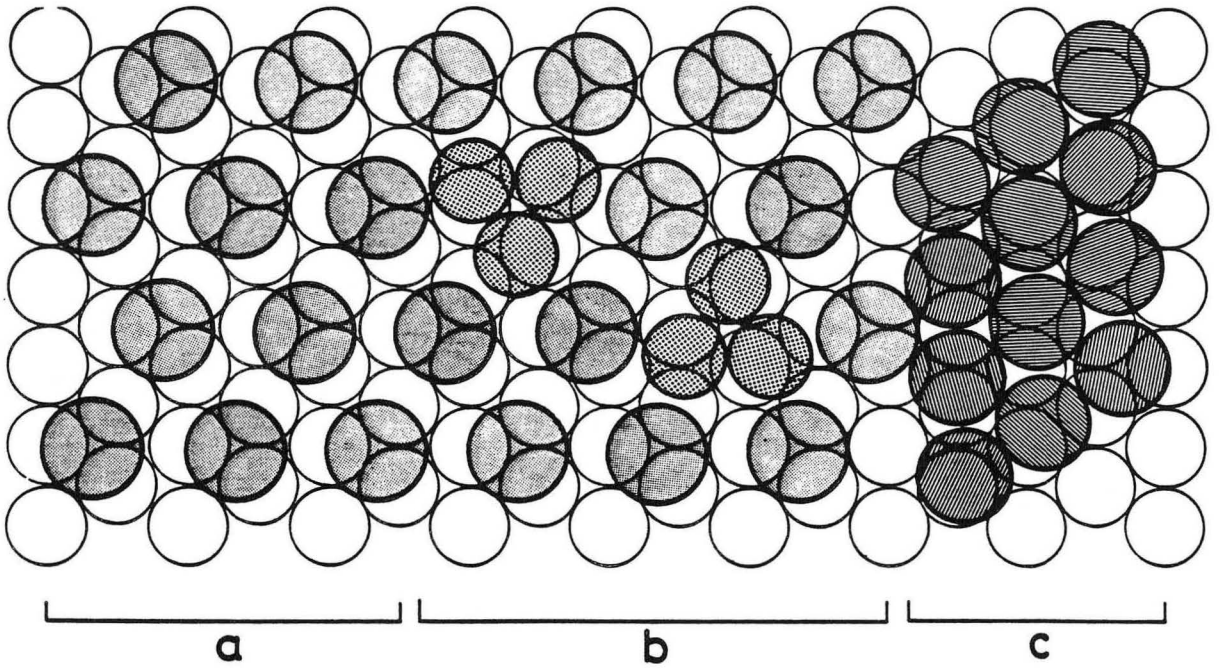

XBL 8110-7089

Fig. 15

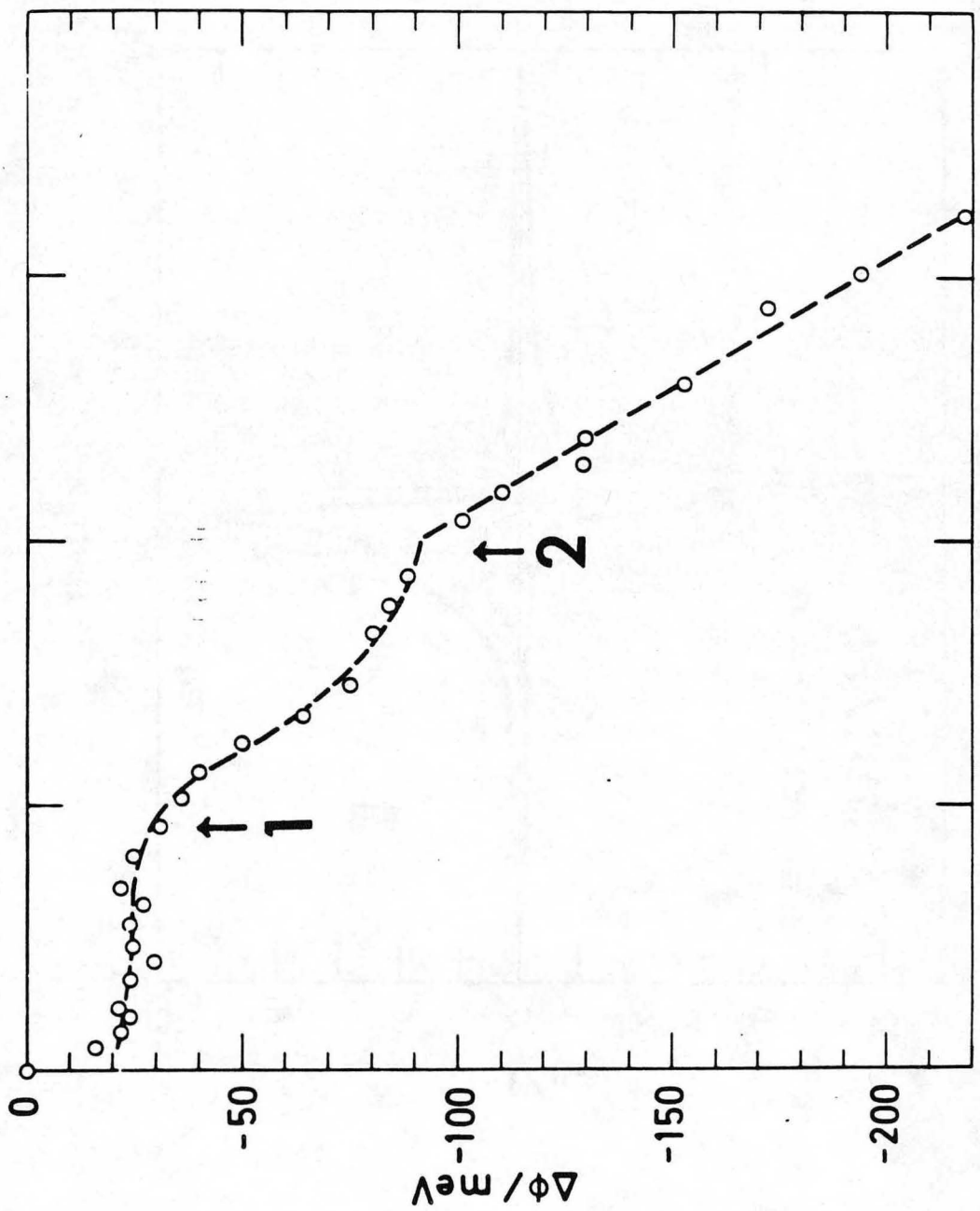
0
-50
-100
-150
-200
Δφ / meV
0
0.25
0.50
0.75
1.00
coverage Θ/ ML
1
2
XBL 8110-7091

Fig. 16

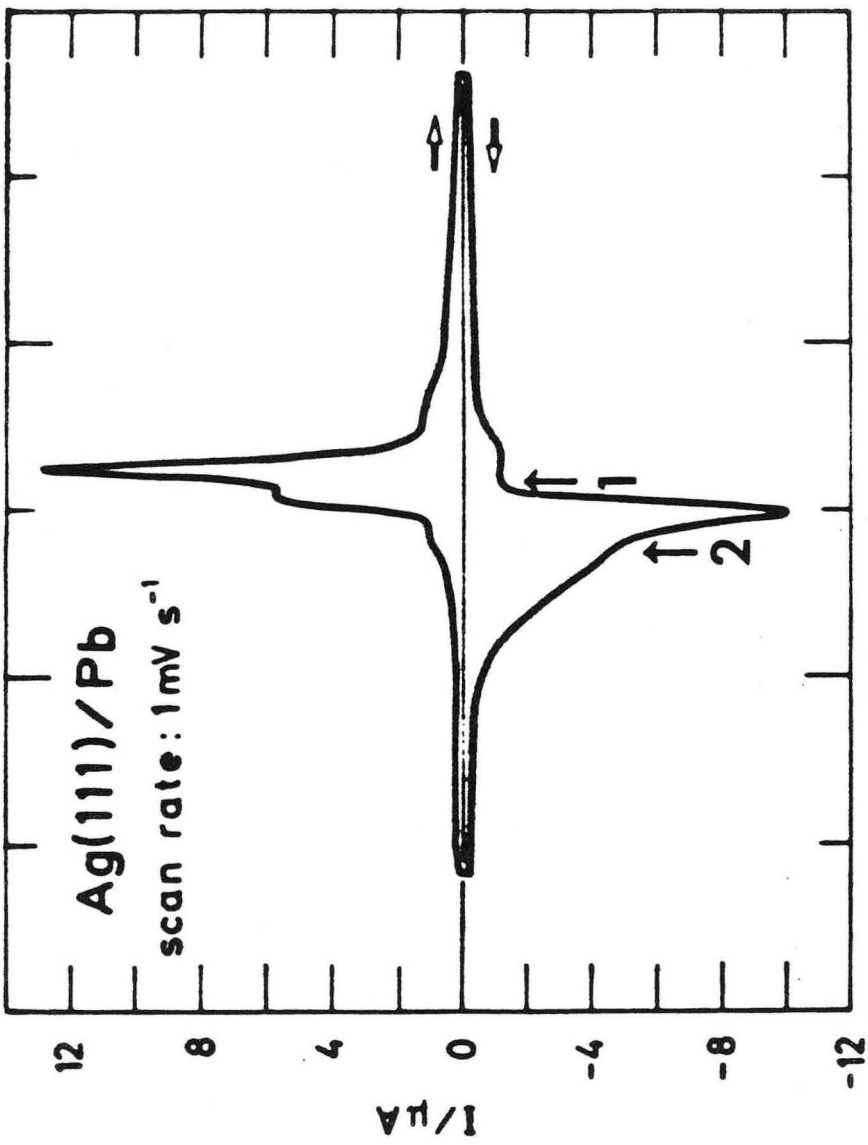

XBL 8110-7088

Fig. 17

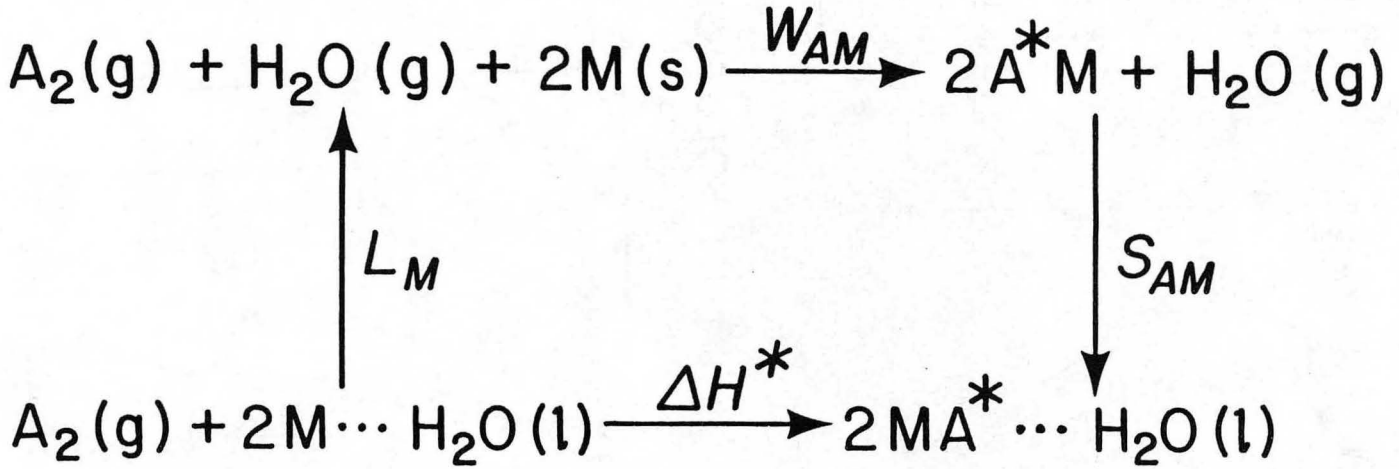

XBL 8110-1381

Fig. 18

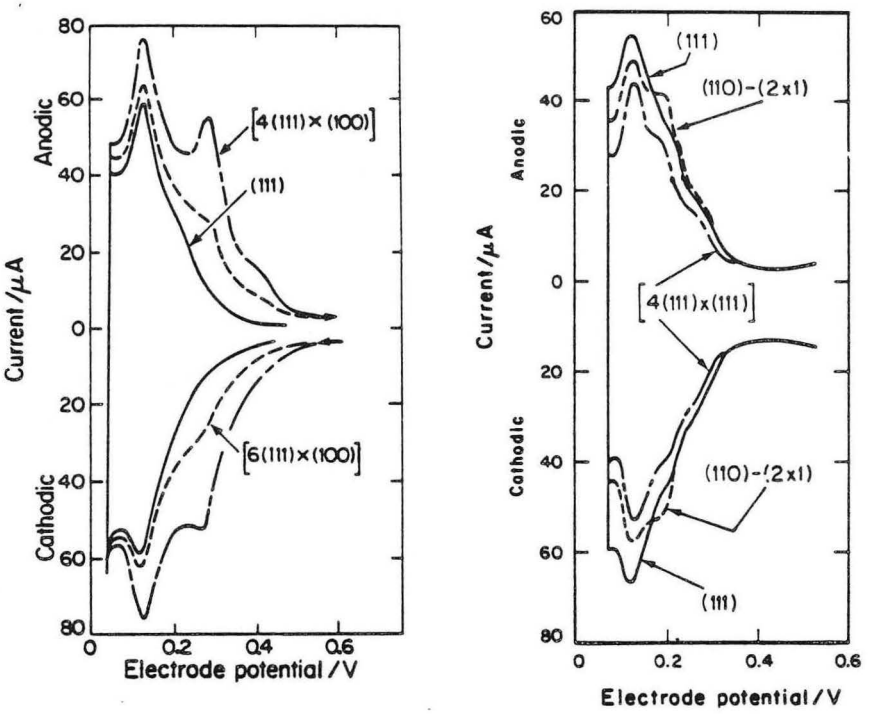

IN SOLUTION

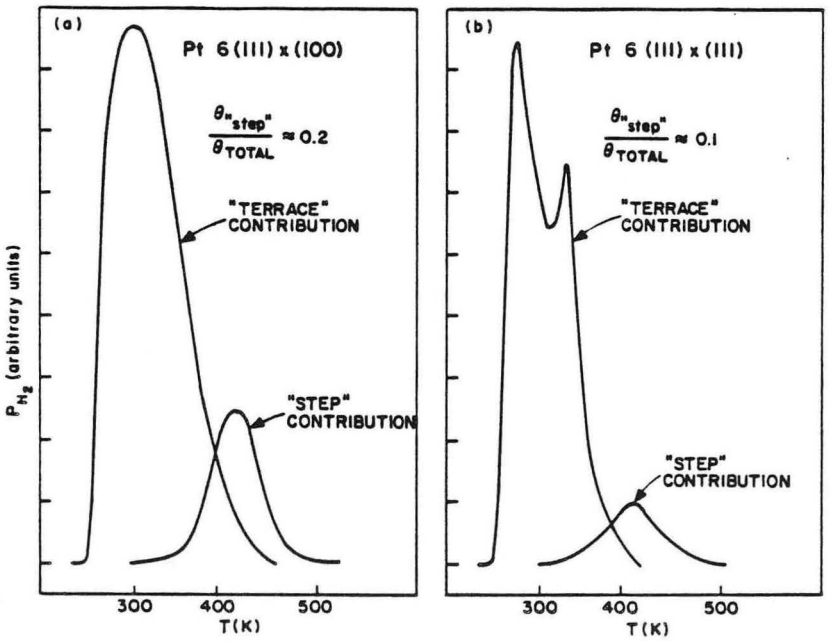

IN VACUUM

XBL 8110-7090

Fig. 19

This report was done with support from the Department of Energy. Any conclusions or opinions expressed in this report represent solely those of the author(s) and not necessarily those of The Regents of the University of California, the Lawrence Berkeley Laboratory or the Department of Energy.

Reference to a company or product name does not imply approval or recommendation of the product by the University of California or the U.S. Department of Energy to the exclusion of others that may be suitable.

TECHNICAL INFORMATION DEPARTMENT
LAWRENCE BERKELEY LABORATORY
UNIVERSITY OF CALIFORNIA
BERKELEY, CALIFORNIA 94720